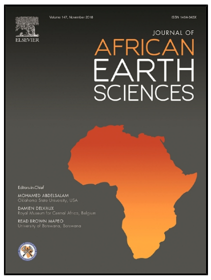

The role of pre-existing Precambrian structures in the development of Rukwa Rift Basin, southwest Tanzania

Obeid Saitabau Lemna, Randell Stephenson, David G. Cornwell

PII:	S1464-343X(18)30296-6
DOI:	10.1016/j.jafrearsci.2018.09.015
Reference:	AES 3327
To appear in:	*Journal of African Earth Sciences*
Received Date:	25 January 2018
Accepted Date:	20 September 2018

Please cite this article as: Obeid Saitabau Lemna, Randell Stephenson, David G. Cornwell, The role of pre-existing Precambrian structures in the development of Rukwa Rift Basin, southwest Tanzania, *Journal of African Earth Sciences* (2018), doi: 10.1016/j.jafrearsci.2018.09.015

The role of pre-existing Precambrian structures in the development of Rukwa Rift Basin, southwest Tanzania

Obeid Saitabau Lemna[a,b], **Randell Stephenson**[a], **David G. Cornwell**[a]

[a]School of Geosciences, University of Aberdeen, Meston Building, King's College, Aberdeen, AB24 3UE, Scotland, United Kingdom

[b]Department of Geology, University of Dar es Salaam, P. O. Box 35052, Dar es Salaam, Tanzania

Abstract

In this study, Shuttle Radar Topography Mission (SRTM) Digital Elevation Model (DEM) and aeromagnetic data are used to analyse the trends of pre-existing basement structures within the Rukwa Rift Basin. The NW-trending Rukwa Rift Basin on the western branch of the East African Rift System, southwest Tanzania, is developing on the NW-trending Paleoproterozoic Ubendian orogenic belt, a belt that experienced multiple orogenic collisions associated with subduction in Proterozoic time and comprises several distinct terranes bounded by faults or shear zones. The results obtained using magnetic edge enhancement (derivatives) methods highlight major magnetic domains identified based on their distinctive magnetic patterns in relation to geology and tectonic setting of the studied area. The results also highlight the Precambrian Chisi shear zone which trends in a NW-SE direction in the subsurface, below the Lake Beds Formation sedimentary succession of the Neogene Rukwa Rift Basin. The orientation of rift border faults and other major faults and their relationship with basement fabrics inferred from SRTM DEM and magnetic data trend mainly NW-SE, which is consistent with those of the NW-trending Paleoproterozoic Ubendian orogenic belt. Thus, Paleoproterozoic Ubendian orogenic belt structures have played a significant role on geometry and orientation of the

Rukwa Rift Basin. These structures facilitated strain localisation within the border faults of the rift basin by exploiting the existence of inherited lithospheric heterogeneity. It can be concluded that the pre-existing faults and shear zones define a mechanical anisotropy in the basement of the Rukwa Rift Basin and facilitated the strain localisation within border fault of the rift.

1. Introduction

Continental rifts are of global importance because they provide a record of the early stages of continental breakup (e.g. Abdelsalam et al., 2004). They are regions of thick sediment accumulation, which provide about 30% of the world's discovered hydrocarbon resources (e.g. Fraser et al., 2007) and most of the geothermal resources in the world are found in regions of active rifts (Şengör, 2011). They generally comprise a group of half and asymmetrical graben of alternating polarities (Laó-Dávila et al., 2015) bounded by border faults. Their initiation and evolution occurs within a heterogeneous lithosphere containing pre-existing (basement) structures that may influence the location and architecture of crustal deformation (e.g. Holdsworth et al., 2001) at different stages of rift development. Therefore, it is essential to characterise pre-existing structures (faults, basement fabrics, shear zones) and examine their complex interplay with extensional tectonic forces to fully understand the evolution of a continental rift (e.g. Aanyu and Koehn, 2011; Katumwehe et al., 2015; Korme et al., 2004).

Regionally, the East African Rift System (EARS; Fig. 1), which is largely controlled by Precambrian basement structures (McConnell, 1972; Morley, 1999; Ring, 1994; Rosendahl, 1987), tends to follow mobile belts that diverge around cratons (Misra and Mukherjee, 2015). The western branch of the EARS is characterised by deep and elongated half graben basins developed within the Precambrian belts (Smets et al., 2015) to the northwest, west and southwest of the Tanzanian Craton (Fig. 2). On a local scale, Katumwehe et al. (2015) demonstrated that the evolution of Albertine-Rhino graben in northwestern Uganda is facilitated by pre-existing Precambrian structures. Using gravity and magnetic data from the Okavango Rift Zone in southwestern Botswana (in southern Africa southwest of the area shown in Figure 1) Leseane et al. (2015) demonstrated that Precambrian structures might result in extensional strain localisation during initiation of continental rifts.

In contrast, there are cases where the observed relationships between basement structures and rift border faults show little or no correlation as regards to the geometry and location of the border fault systems (Daly et al., 1989; Ebinger et al., 1987). In these settings, it is more likely that continental rift development is controlled by deeper structures originating from the lithosphere (Delvaux et al., 1999; Kinabo et al., 2007), an assertion recently strengthened by numerical modelling studies (Heron et al., 2016). In any case, understanding the influence of pre-existing structures in strain localisation is, for example, important for seismic hazard assessment along continental rifts (Dawson et al., 2018; Kolawole et al., 2018, 2017).

Magmatism is a widely observed phenomenon associated with continental rifting such as the eastern branch of the EARS. Numerical modelling studies demonstrate the role of magma in softening and facilitating the stretching of the lithosphere and strain localisation during rifting (Bialas et al., 2010; Buck, 2006;

Schmeling, 2010). Extension due to magma intrusion has been observed in the eastern branch of EARS, specifically in the Main Ethiopian Rift (Ebinger and Casey, 2001), the northern Afar Depression (Wright et al., 2006) and in the Natron Rift in northern Tanzania (Calais et al., 2008; Kampunzu et al., 1998); however, magmatism in the western branch of the EARS is observed only in small outcrops occupying the tips of some rift segments (Kampunzu et al., 1998).

The Rukwa Rift Basin, southwestern Tanzania, lies between lakes Tanganyika and Nyasa/Malawi (Kilembe and Rosendahl, 1992) in the western branch of the EARS and is underlain by the NW-SE trending Precambrian crystalline rocks of the Paleoproteroic Ubendian orogenic belt (Figs. 1-3). The Ubendian orogenic belt is characterised by eight lithological terranes separated by the NW-trending ductile shear zones (Daly, 1988). These pre-existing structures (shear zones) may have been reactivated at depth during rifting, acting as planes of weakness (Daly et al., 1989; Dawson et al., 2018; Kolawole et al., 2018), and therefore the Rukwa Rift Basin is an ideal setting to explore the complex relationship between basement structures and continental rift evolution.

An integrated interpretation of aeromagnetic and topographic data is presented here aimed at establishing the geological expression of Precambrian faults/lineaments in the basement of the Rukwa Rift Basin in order to investigate the role played by these pre-existing structures on the development of NW-SE trending Rukwa Rift Basin.

2. Geology and tectonic setting

2.1 The East African Rift System (EARS)

The East African Rift System (Chorowicz, 2005) is considered as a classical example of an intraplate active divergent zone, at an early stage of continental rifting (e.g. Daly et al., 1989; Simiyu and Keller, 2001) with the exception of Afar Depression which may be transitioning into an oceanic spreading centre (Bastow et al., 2011; Bridges et al., 2012; Reed et al., 2014). The EARS goes southwards from the Afar Depression in Ethiopia (Beyene and Abdelsalam, 2005) as the Main Ethiopian Rift until it reaches the area of the Aswa Shear Zone (ASZ; Fig.1), a Neoproterozoic structure (Saalmann et al., 2016), where it divides into two main branches, the eastern and western branches, respectively (Fig. 1).

These two branches bifurcate with the Archaean age Tanzanian Craton between them (Fig. 2) and follow Proterozoic mobile belts (e.g. Ring et al., 2005), indicating that the EARS may have formed according to large scale zones of weakness in the lithosphere (Ring and Betzler, 1995). The eastern branch in Tanzania splits into three segments, namely the Eyasi segment to the west, Manyara segment to the middle and Pangani segment (Fig. 1) to the east (Mulibo and Nyblade, 2016). Note that the eastern branch is not described or discussed further in this paper since it is not the focus of the present study. The western branch of the EARS runs from Albertine-Rhino grabens (Fig. 2) (Katumwehe et al., 2015) in Uganda south through Lakes Tanganyika, Rukwa (the main focus of this study), and Nyasa/Malawi (Chorowicz, 2005) to the Mozambique coastal plain (Fig. 1). It is described in more detail in the following sections.

2.2 The western branch of the EARS

The western branch of the EARS is more seismically active than the eastern branch (Chorowicz, 2005; Mulibo and Nyblade, 2016). It has a length of approximately 2100 km from the Albertine-Rhino grabens (Chorowicz, 2005; Katumwehe et al., 2015) in the north through the Kivu graben and Tanganyika Rift (Ebinger, 1989a; Smets et al., 2016; Wood et al., 2017), which are represented by lakes Albert, Edward, Kivu and Tanganyika on Figure 2. To the southeast it continues into the Rukwa Rift Basin and then enters the Malawi Rift in the south (lakes Rukwa and Malawi/Nyasa on Figure 2).

The western branch is generally considered magma poor (Kampunzu et al., 1998) with the exception of few documented volcanic centres in Virunga, Toro-Ankole, Mwenga-Kamitunga, Bukavu (Fig. 2) and Rungwe Volcanic Province (RVP; Figs. 2 and 3(a)). The last lies within the study area and separates the NW–trending Rukwa Rift Basin, the N-trending Nyasa (Malawi) Rift and the NE-trending Usangu Basin. It has been interpreted as forming within an accommodation zone between the Rukwa, Nyasa (Malawi) and Usangu rift segments by normal faulting within a semi-radial extensive stress field (Ebinger et al., 1989; Fontijn et al., 2010). The Usangu Basin is developing at a right angle to the strike of the Rukwa Rift Basin (Chorowicz, 2005; Harper et al., 1999; Le Gall et al., 2004).

The western branch of the EARS is generally thought to be younger than its eastern counterpart, with the onset of rifting being about 12 Ma (Ebinger, 1989b; Kampunzu et al., 1998). However, recent studies based on U–Pb and $^{40}Ar/^{39}Ar$ dating of volcanic tuffs within the Rukwa Rift Basin, U–Pb detrital zircon geochronology and palaeocurrent analysis of ancient rivers suggest that the onset of rifting may be as old as about 25 Ma contemporaneously with the eastern branch of the EARS in Kenya(Roberts et al., 2012).

2.3 Rukwa Rift Basin

The Rukwa Rift Basin is a NW-SE trending segment of the western branch of the EARS, approximately 300 km long and 50 km wide (Roberts et al., 2004). It is situated in southwestern Tanzania between lakes Tanganyika and Nyasa/Malawi (Figs. 1 and 2). The central part of the basin, about one-third of it, is occupied at present by Lake Rukwa, a shallow (<15 m deep) lake (Morley et al., 1999; Roberts et al., 2010). The long, linear Lupa Fault and the more southerly striking scarp of the Ufipa Fault bound the rift on its northeastern and southwestern flanks, respectively (Fig. 3(a)). The Lupa Fault is well defined in the northwestern part of the study area where the interpretation of gravity and seismic data indicate a listric fault with a throw of 7 km (Morley et al., 1999; Peirce and Lipkov, 1988).

The asymmetrical morphology of the Rukwa Rift Basin, lying on the southwestern flank of the Ufipa escarpment, is shown by the topographic profile seen in Figure 3(b). The Rukwa Rift Basin splits into two branches at its southern end; the Songwe trough and the Msongano trough, separated by the Mbozi terrane (Fig. 3(a)). In the southeast, the Ufipa Fault bounds the Msongano trough, trends in NW–SE direction and turns to the WNW to form the Chisi escarpment (Fernandez-Alonso et al., 2001; Kervyn et al., 2006) (Fig. 3(a)). The rift is surrounded and underlain by basement rocks (Kilembe and Rosendahl, 1992; Morley et al., 1999; Roberts et al., 2010) of the Paleoproterozoic Ubendian orogenic belt on the western side of the Archaean Tanzania Craton (Fig. 3(a)). The rocks of the Ubendian orogenic belt consist of the high grade metavolcanics and metasediments, granulites, amphibolites, gneisses, schists and quartzites (McConnell, 1950).

Stratigraphic records show deposition of tectonically controlled sedimentary successions during the Permian, Cretaceous, Paleogene, and Neogene-Quaternary (Dypvik et al., 1990; Roberts et al., 2010, 2004), These episodes include: (1) a Permo-Triassic extensional event that resulted in the deposition of Karoo Supergroup (Kilembe and Rosendahl, 1992); (2) a Cretaceous rifting event that resulting in the deposition of fluvial lower Red Sandstone Group depositional sequence (Roberts et al., 2010, 2004); (3) a late Oligocene event resulting in the deposition of fossiliferous fluvio-lacustrine upper Red Sandstone Group depositional sequence (Roberts et al., 2012, 2010, 2004); and (4) a late Miocene to Recent rifting event and deposition of the Lake Beds Formation. The Lake Beds are thicker near the Lupa border fault at ~4 km (from seismic reflection data) (Kilembe and Rosendahl, 1992), consist of unconsolidated green greyish sands, silts and clays and unconformably overlie the Red Sandsone Group. Seismic reflection data show that the maximum thickness of the sedimentary fill of the Rukwa Rift Basin varies from 2 km in the northwest to 7 km in the southeast (Kilembe and Rosendahl, 1992; Mbede, 1993; Morley et al., 1999).

2.4 Precambrian structures and basement rocks around the Rukwa Rift Basin

The NW-trending Paleoproterozoic Ubendian orogenic belt is developed at the southwestern margin of the Tanzanian Craton and has been subdivided into eight lithological blocks separated by ductile shear zones that trend in a NW-SE direction (Daly, 1988). One such shear zone is the NW-trending Mughese shear zone (Fig. 2) within the Ufipa terrane (Fig. 3(a)) separating the Ubendian orogenic belt from the Archaean – Paleoproterozoic Bangweulu cratonic block (Boniface and Schenk, 2012; Fritz et al., 2013; Ring et al., 2002).

This Ubendian orogenic belt has experienced a number of different episodes of tectonic reactivation, including three dominantly ductile ones in the Precambrian and two well expressed brittle reactivation phases before the onset of Meso – Cenozoic Rukwa rifting (Boniface et al., 2012; Boniface and Schenk, 2012; Delvaux et al., 2012; Klerkx et al., 1998; Lenoir et al., 1994; McConnell, 1972, 1950; Roberts et al., 2010; Theunissen et al., 1996; Tiercelin et al., 1988).

The first phase of predominantly ductile deformation (2100–2025 Ma) is recorded by granulite-facies metamorphism displaying an E–W to WNW–ESE foliation (Lenoir et al., 1994). and is thought to have occurred during orogenic collision of the Tanzanian and Congo cratons (Muhongo et al., 2002). The second ductile phase (1950–1850 Ma) (Theunissen et al., 1996) produced NW–SE trending dextral shear zones that are expressed only in the Paleoproterozoic Ubendian orogenic belt (Theunissen et al., 1996). It is linked with northwards thrusting in the Usagaran belt south of the Tanzanian Craton (Fig. 2) as well as late- to post-orogenic (c. 1860 Ma) granitic intrusions (Aanyu and Koehn, 2011; Lenoir et al., 1994). This date (1860 Ma) accordingly marks the youngest expression of the second phase of deformation (Lenoir et al., 1994), although there is local evidence of tectonic reactivation at ca. 1725 Ma (Lenoir et al., 1994). The third deformation episode occurred in the Neoproterozoic (ca 750 Ma) and is expressed as the reactivation of the NW-SE orientated (second phase) Ubendian shear zones and is interpreted as evidence of a “sinistral transpression regime”

(Lenoir et al., 1994). It exhibits brittle and ductile shearing, retrograde metamorphism and alkaline igneous intrusions (Basu and Ikingura, 1984; Lenoir et al., 1994; Stendal et al., 2004).

To the northeast and southwest, the Rukwa Rift Basin is surrounded and underlain by the uplifted blocks of the Katuma, Ubende, Wakole, Ufipa and Lupa terranes respectively (Fig. 3(a)). The Katuma block/terrane of the northestern Ubendian orogenic belt is subdivided into two groups (Kazimoto et al., 2015 and references therein), namely the Katuma Group consisting of metamorphosed igneous rocks and the Ikulu Group consisting of metamorphosed sedimentary rocks. Kazimoto et al. (2014) consider that the rocks of the Katuma Group are of Neoarchaean (2.71–2.64 Ga) and/or Paleoproterozoic (2.02–1.94 Ga).

The Ubende terrane is characterised by mafic gneisses hosting mylonitic eclogites, as well as other kinds of gneisses, locally, as well as granulites (Boniface et al., 2014 and references therein).

The Wakole terrane is bounded by mylonitic shear zones (Boniface et al., 2014; Daly, 1988; Theunissen et al., 1996). It is composed dominantly of biotite-garnet-kyanite-schists though quartzites and gneisses also occur (Boniface et al., 2014).

The Ufipa terrane is dominated by granitic and granodioritic rocks. Its structural grain is characterised by NW-SE oriented amphibolite facies gneissic layering. Thin mylonite sequences are observed along steeply inclined and tightened limbs of the NW trending ductile folds of the Ufipa gneisses indicating sinistral stike-slip wretch faulting (Theunissen et al., 1996). On the western side of the Ufipa terrane, the ductile Ufipa gneisses are separated from the highly sheared Kate-

Kipili sequences by sinistral strike-slip mylonites (Theunissen et al., 1996). To the south of this terrane, along the Ufipa Fault (Fig. 3(a)), a similar zone of reactivation forms the boundary between the Mbozi and Ufipa terranes (Fernandez-Alonso et al., 2001). Likewise, the Kanda Fault (Fig. 3(a)), an active fault within the Ufipa terrane (Delvaux et al., 2012, 1998), overlies a mylonitic shear zone observed in the limb of tightly folded Ufipa gneiss (Delvaux et al., 2012; Fernandez-Alonso et al., 2001; Theunissen et al., 1996; Vittori et al., 1997).The Lupa terrane is also dominated by high-grade metamorphic rocks (Manya, 2014) that are intruded by a variety of younger igneous rocks including mafic dykes (Lawley et al., 2013; Manya, 2014; Mnali, 1999).

In its southern segment, the Rukwa Rift Basin is flanked by the Mbozi and Upangwa terranes. The Mbozi terrane forms a plateau at the southeastern end of the Rukwa Rift Basin bounded by the Songwe trough to the northeast and the Msongano trough to the southwest. It is composed mainly of mafic and ultramafic granulites and gneisses. Theunissen et al. (1996) observed NW oriented sinistral strike-slip mylonites within this terrane, where they alternate with high grade gneisses and granulites. The Upangwa terrane mainly comprises anorthosite massifs in the north and, in the south, high grade gneisses (Theunissen et al., 1996). The gneissic layering in this terrane dips steeply to the west, trending WNW-ESE to NW-SE (Theunissen et al., 1996).

3. Data and Methods

3.1 SRTM Data and DEM Lineament Analysis

Shuttle Radar Topography Mission (SRTM) Digital Elevation Model (DEM) (Fig. 4) with a spatial resolution of 30 m (Farr et al., 2007) is used to delineate rift related faults and lineaments in the study area. Following the methodology of Smets et al. (2016), hillshade (shaded relief) and slope images were derived from these data for analysis. Hillshade provides information on slope aspect and helps in the interpretation of structures and morphological characteristics of relief but choice of illumination may mislead interpretation (Smets et al., 2016). Slope images generally highlight rapid changes at the base and the top of a slope: concave at the base and convex at the summit allowing a clear indication of breaks of slope and ridges (Smith and Clark, 2005). In this study, Multidirectional Oblique Weighted (MDOW) (Mark, 1992; Smets et al., 2016) hillshade images were produced using the ArcGIS extension DEM Surface Tools (Jenness, 2013). MDOW emphasises oblique illumination on all surfaces whereby the shaded-relief images are illuminated from 225°, 270°, 315°, and 360° azimuth and a sun elevation of 45˚ (Mark, 1992). Figure 5 illustrates these images for part of the study area. The extraction of topographic lineaments can be achieved either manually or automatically, such as using an edge-detection technique. In this study, manual extraction was preferred because it allowed the user to include geological information during extraction and interpretation (Mshiu et al., 2015), which is not possible during automatic extraction. Faults and/or lineaments were extracted using elevation, slope and hillshade images combination of (Fig. 5(d)) by manual digitization onscreen as described by Kumanan et al. (2011) and Ramli et al. (2010). The abrupt change in colour (tonal patterns), topographical scarps and linear drainage patterns (Mshiu et al., 2015; Smets et al., 2016) were used as a proxy for the identification and extraction of faults and or lineaments. Therefore, lineaments of at least 5 km in length were picked at the lower break of slope of straight topographical escarpments and the morphology of river channels, which are assumed to be straight where they coincide with fault traces but meandering elsewhere (Smets et al., 2016). The extracted lineaments have been superimposed in Fig. 5(d). Google Earth imagery and topographical maps were used during extraction and interpretation to prevent inclusion of man-made features such as roads and transmission lines as suggested by Mshiu et al. (2015).

3.2 Magnetic data

3.2.1 Data transformation and filtering

The aeromagnetic dataset used in this study is part of a regional airborne dataset acquired by Geosurveys International in 1977 and 1980 and provided by Tanzania Petroleum Development Corporation (TPDC). The data were acquired at a flight altitude of ~120 m at 1 km line spacing and 10 km tie line spacing oriented E-W.

Total magnetic intensity (TMI) data were gridded using minimum curvature methods described by Swain (1976) and Briggs (1974). A grid cell size of 200 x 200 m, one-fifth of the survey line spacing, was adopted to preclude artefacts perpendicular to the line direction (Anudu et al., 2014; Dentith, 2011).

The TMI grid data were then reduced to pole (RTP) (Baranov, 1957; Blakely, 1995), which removes the latitude derived shift of anomalies from the centre of their magnetic sources which help to relate/correlate magnetic anomalies with geological information. Parameters used in the RTP filter were geomagnetic inclination of -41.4° and geomagnetic declination of -3.2°. The geomagnetic inclination and declination are the mean values computed based on the IGRF-3 model for the year 1980, which corresponds to the magnetic field at the time of the airborne survey. A 1 km upward continuation filter was applied to magnetic data in order to reduce the noise and aid delineation of deeper structures (Jacobsen, 1987). To assist in determining deep magnetic sources, matched bandpass filters based on the method of Phillips (2001) were used. Matched bandpass filtering separates potential-field data (gravity and magnetic) into anomalies from different wavelength components (taken to indicate different source depths) (Phillips, 2001). In this study, a cut-off wavelength of about 7000 m was used, which corresponds to anomalies originating at a depth of about 6 km. This wavelength was chosen based on the power spectrum curve seen in Figure 6(a).

This was implemented by utilising the response of a four-layer model (three dipole layers overlying a magnetic half space) matched to the radially symmetric component of the observed magnetic field power spectrum (Phillips, 2001). The observed and computed power spectra and bandpass filters obtained during filtering are shown in Figures 6(b) and 6(c) respectively.

The filtered matched bandpass RTP-TMI anomaly map seen in Figure 6(c) was then used as the basis for edge detection/filtering/enhancement techniques presented in the following section below.

3.2.2 Magnetic anomaly enhancements

The total horizontal derivative filter (THDR) (Cordell and Grauch, 1985; Phillips, 2002) was applied to matched bandpass filtered RTP-TMI grid data (Fig. 6(c)) in the wavenumber domain (Geosoft Inc., 2011) in order to image the edges of magnetic bodies within the study area. The results are presented in Fig. 7. This filter is considered as a good edge detection filter because it is less sensitive to short-wavelength noise in the data because it only requires the two first-order horizontal derivatives of the magnetic field (Phillips, 2002).

The tilt angle derivative (TDR) (Miller and Singh, 1994; Verduzco et al., 2004), which is a normalized derivative based on the ratio of the vertical derivative and horizontal derivatives of RTP field, was applied to the match filtered RTP-TMI grid data in order to evaluate the dip of Precambrian basement structures. The results are presented in Figure 8. To examine the spatial extent and horizontal continuity of the magnetic anomalies, a positive tilt derivative map was extracted from the tilt derivative anomaly map (Fig.8). The results are shown in Figure 9. All the calculated values of the TDR are restricted to $\pm\frac{\pi}{2}$. The advantage of this filter is that positive values are obtained within the magnetic source whereas the negative angle values indicate tilt variations outside the magnetic source region (Miller and Singh, 1994) and it is effective in mapping magnetic features/edges that are subtle and less evident in other drivative filters like the horizontal and vertical derivatives (Katumwehe et al., 2015; Kolawole et al., 2018). These filters were chosen because they have been proven to be effective in mapping subsurface structural edges associated with both strongly and weakly magnetised bodies (Dawson et al., 2018; Fairhead et al., 2011; Kolawole et al., 2018). Faults and/or lineaments from aeromagnetic data were extracted using the curvature analysis method (Blakely and Simpson, 1986; Phillips et al., 2007). The orientation of the extracted faults/lineaments were plotted on rose diagrams using Polar Plots for ArcGIS extension developed by Jenness (2014).

4. Results and discussion

4.1 SRTM DEM basement fabrics and magnetic character of the study area

Figure 10(a) shows a structural map constructed from the edge enhancement (derivatives) of the RTP-TMI magnetic data with the SRTM DEM data superimposed for the study area as a whole. Lineament trends of these are shown as rose diagrams in Figures 10(b) and 10(c). These data have been used to define five magnetic domains within the study area, on the basis of geology and tectonic setting, as shown in Figure 7 (areas A-E). The structures/magnetic lineaments of each of these are discussed below in terms of the geological map seen in Figure 3.

Domain A (Figs. 7 and 11) in the northern part of the study area is dominated by long, narrow N-S trending magnetic anomalies superimposed in a more chaotic anomalies associated with basement rocks. These magnetic anomalies are more pronounced in the TDR (Fig. 8), which defines the contacts and edges of geological features with alternating high and low magnetic susceptibilities. The spatial extent and continuity of these magnetic anomalies are clearly visible on the positive TDR image in Figure 9. The long and narrow N-S trending magnetic anomalies (Fig. 11(b and c)) are interpreted to be caused by Precambrian dolerite dyke swarms, which do not crop out on the surface. The anomalies are part of the long, narrow, and linear magnetic anomalies that run northwards almost as far as Lake Victoria (cf. Marobhe, 1989). This domain is part of the Tanzanian Craton (Figs. 3), which consists of dioritic to granodioritic rocks and orthogneisses (Kabete et al., 2012; Thomas et al., 2016). The orientation of the lineaments extracted from curvature analysis method is shown in a rose diagram in Figure

11(d). The only other prominent trend in this domain reflects the NW- SE trending magnetic lineaments (Fig. 10(b and c)), also seen in the SRTM DEM data (Figure 11(a)), that are cross-cut by the N-S trending dyke swarms.

Domain B (Figs. 7 and 12) in the northwestern part of the study area is characterised by strong NW-trending SRTM DEM and magnetic fabrics/lineaments (Figs. 8, 9 and 12(a-c)). This domain corresponds to the NW trending rocks of the Katuma, Wakole, and Ubende blocks/terranes and the northern part of the Ufipa terrane. This region constitutes part of the Meso- and Neoproterozoic sedimentary rocks found along ductile shear zones as a result of repeated sinistral wrench fault reactivations. The rose diagram of lineament trends for this domain (Fig. 12(d)) clearly reflect the faults and shear/suture zones mapped from previous field and geological studies (Boniface and Schenk, 2012; Daly, 1988; Delvaux et al., 2012; Lenoir et al., 1994). The weakly indicated N-S trend anomalies (Fig. 12(d)) may be due to the same mafic dyke swarms known to occur in domain A.

Domain C (Figs. 7 and 13) is characterised by isolated circular and elongated magnetic anomalies. NE-SW and E-W trending structures delineated from SRTM DEM data (Fig. 13(a)) and magnetic fabrics delineated from magnetic anomalies (Fig. 13(b-c)) are also observed in this region. The magnetic anomalies observed in this region corresponds the high-grade metamorphic rocks of the Lupa terrane (Fig. 3(a)). The eastern part of this domain is characterised by relatively smooth (low amplitude) magnetic anomalies (Fig. 13(b)) that correlate with sediments filling the Usangu Basin. High amplitude magnetic anomalies are observed in the southern part of this domain. This group of anomalies may be correlated with mafic-ultramafic intrusive rocks observed in this region. Other prominent features are N-S trending magnetic lineaments that are caused by the mafic dyke swarms similar to the observed magnetic lineaments in domain A (Fig. 11(b)). In general, the magnetic patterns observed in this domain do not show a preferred orientation (Fig. 13(d)).

Domain D (Figs. 7 and 14) corresponds to part of the NW-trending strata of the Ufipa terrane and part of the sedimentary rocks within the Rukwa Rift Basin. Strong NW- SE trending lineaments delineated from SRTM DEM data (Fig. 14(a)) and those delineated from magnetic anomalies (Fig.14(b and c)) dominate the former with relatively low amplitude magnetic anomalies correlating with the later and this trend is clearly expressed in the rose diagram for this domain (Fig. 14(d)). The Ufipa terrane consists of NW elongated Neoproterozoic eclogites, biotite gneisses metapelites and schists. In the northeastern and southwestern part of this domain, the NW-trending magnetic anomalies coincides with the NW–trending Lupa Fault and the NW-trending Ufipa fault scarp respectively (Figs. 3 and 14(b)). The former is the main border fault of the Rukwa Rift Basin.

Domain E (Figs. 7 and 15) in the southern part of the study area consists of high amplitude magnetic anomalies trending in NW-SE direction. This group of anomalies are due to mafic ultamafic rocks of the NW- SE trending Mbozi block. The trends of structures mapped from SRTM DEM data and those delineated from magnetic anomalies in the Mbozi block trend in a NW–SE direction (Fig. 15(a-c)). The rose diagram (Fig. 15(d)) indicates a weak more or less N-S trend, possibly correlating with similarly trending mafic dykes that have been mapped in this area (Brock, 1961). In general, the rocks that comprise this block are strongly foliated and sheared, and faulting generally follows the strike of pre-existing foliations.

In general, the principal magnetic anomalies in the Rukwa Rift Basin reflect the location of the crystalline Precambrian basement rocks, sedimentary rocks and Cenozoic volcanic rocks. Comparison of the magnetic anomalies with geological features of the region and trends of the structures mapped from SRTM DEM data shows that positive magnetic anomalies are located in areas with basement outcrops and thin unconsolidated sediments. These positive anomalies generally trend NW-SE (Figs. 7-15), an indication that they are associated with basement features/mineralogical composition in the study area. Earlier regional interpretations of geology, SRTM DEM, (e.g. Delvaux et al., 2012; Fernandez-Alonso et al., 2001; Theunissen et al., 1996) gravity and magnetic data (Marobhe, 1989; Peirce and Lipkov, 1988) also recognised these trends. Both the northeast and southwest border faults of the Rukwa Rift Basin coincide with NW-trending magnetic fabrics defined by alternating high and low magnetic anomalies (Figs. 7-9 and 13(b)). The Rukwa Rift Basin itself is represented by broad, long wavelength magnetic anomalies, an indication of its sedimentary infill. Individual magnetic lineaments show correlation with geologically mapped lithologies, shear zones, and faults (Figs. 3 and 7-8), mostly trending in a NW-SE direction. This direction is the primary direction of many of the structural features of the Paleoproterozoic Ubendian orogenic belt.

4.2 Precambrian basement and rift structures

In this section, the relationship between the pre-existing basement structures and rift related structure is examined by comparing structures interpreted from SRTM

DEM data and aeromagnetic anomalies in the direct vicinity of the Rukwa Rift Basin. This is the first study that has utilised combined topographic and magnetic datasets to illuminate the relationship between basement and rift structure around the Rukwa Rift Basin. The alignment of dominant rift structures with basement fabrics inferred from the magnetic data, augmented by the trends extracted from STRM DEM data (Fig. 10(b and c)), strongly confirms that the geometry and orientation of the Rukwa Rift Basin is controlled or at least strongly influenced by basement structures of the NW-trending Paleoproterozoic Ubendian orogenic belt. From north to south, the Rukwa Rift Basin strikes NW-SE, a direction which is parallel to the regional structural orientation of the Paleoproterozoic Ubendian orogenic belt (Figs. 2 and 3(a)). This belt is a linear, NW-SE trending strike-slip faults and is part of a large Paleoproterozoic orogeny, developed around the west and southwestern margin of the Archaean Tanzanian Craton (Fritz et al., 2013; Lenoir et al., 1994). The magnetic lineaments extracted from derivative filters and plotted on the rose diagram (Fig. 10(b)) show the dominant orientation of pre-existing structures around the Rukwa Rift Basin. Within the Ubendian orogenic belt, the magnetic fabrics are dominated by the NW-trending structures. The orientation of these structures derived from magnetic data shows how these complex pre-existing structures of the Paleoproterozoic Ubendian orogenic belt controlled the orientation and geometry of the Rukwa Rift Basin.

4.3 Relationship between Rukwa Rift Basin Border Faults and basement fabrics

Both the northeastern and southwestern border faults (i.e., Lupa and Ufipa faults respectively) coincide with NW trending magnetic fabrics defined by magnetic highs and lows (Fig. 7). These NW-trending magnetic anomalies dip to the SW and NE, respectively (Fig. 8). The SW dipping magnetic fabrics correspond to the northeastern border fault of Rukwa Rift Basin (Lupa Fault) while the NE dipping patterns correspond to Ufipa Fault scarp. The spatial extent and continuity of the magnetic anomalies are clearly visible in the positive TDR map (Fig. 9). This image shows the extent and continuity of magnetic anomalies, especially the high magnetic anomaly of the region. Relating the structural trends extracted from SRTM DEM data and plotted on rose diagram (Fig. 10(c)) and lineaments extracted from aeromagnetic data (Fig. 10(b)) shows a nearby parallelism between the northeastern and southwestern border faults of the Rukwa Rift Basin with the pre-existing Precambrian structures, demonstrating that the overall trend of the rift is controlled by pre-existing basement structures. Seismic reflection studies suggest that the Lupa Fault at one time comprised of three separate faults that subsequently merged together to form a single and a continuous fault of over 200 km (Morley et al., 2000). This fault parallels the NW-trending pre-existing Precambrian basement fabrics and shear zones that may have been reactivated during rifting. The reactivation of pre-existing Precambrian basement fabrics and/or shear zones within the Lupa Fault facilitated the strain localisation within the Lupa Fault in order to develop as the main northeastern border fault of the Rukwa Rift Basin. This fault is a weak zone/reactivation zone along the contact between the Ubendian orogenic belt and the Tanzanian Craton (Fernandez-Alonso et al., 2001). The parallelism between the border faults of the Rukwa Rift Basin and structural trends of the Ubendian orogenic belt (cf. Fig. 14(a-c)) is often considered as an example of a rift reactivated steep basement shear zone, "resurgent tephragenic lineament" (McConnell, 1980), "perennial long lived structural weakness" (Sutton and Watson, 1986), or as "a zone of lateral shear transfer" (Daly, 1988).

The Lupa Fault is well defined in the northwest part of the study area where the interpretation of gravity and seismic data indicate a listric fault with a throw of 7 km (Morley et al., 1999; Peirce and Lipkov, 1988). To the southeast of the study area (Fig. 3(a)), this fault becomes difficult to follow within the metasediments of the Mbeya Range hills, bounded on their southwest by the Mbeya Range Fault and it disappears entirely in the volcanic sediments of the Rungwe Volcanic Province. The present analysis of aeromagnetic data shows a continuous lineament, which correlates in part with the Lupa Fault (Fig. 9) as defined and which can be traced further through the Rungwe Volcanic Province. This indicates that there is a possible direct link between the Lupa Fault and the Livingstone Fault (Fig. 4), which is the northeastern border fault of the Nyasa/Malawi Rift Basin as has been suggested by Marobhe (1989). Both the Rukwa Rift Basin and the sedimentary infill of the northern Nyasa/Malawi Rift thickens to their northeast sides, which are bounded by the Lupa and Livingstone faults, respectively (Flannery and Rosendahl, 1990; Kilembe and Rosendahl, 1992; Morley et al., 1999). The Lupa-Livingstone Fault system was established as early as the Karoo times and it is believed that it may have been rejuvenated during the Mesozoic (Delvaux and Hanon, 1993). If the Lupa-Livingstone fault system is continuous but obscured by younger RVP volcanics, it could be that it provided the conduit for these volcanics. This is compatible with Kampunzu et al.'s (1998) assertion that the age of early volcanism in the RVP is ~9 Ma, several million years younger than the Rukwa Rift Basin and formation of its border faults. One anomalous aspect observed on the Lupa-Livingstone fault system is that the scarp of the Livingstone Fault is higher than that of the Lupa Fault. The most possible explanation for this may be that the Lupa Fault scarp was more significantly modified during a longer period of erosion as suggested by apatite fission track results (Mbede, 1993; van der Beek et al., 1998). Another possible explanation is that the high topography of the Livingstone Fault may be due to regional isostatic response to erosion of the escarpment or the Livingstone Fault was exhumed at a faster rate than the Lupa Fault during Cenozoic rifting.

The Ufipa Fault scarp (southwestern border fault of the Rukwa Rift Basin) lies within a terrane-bounding NW-trending mylonitic shear zone called the Mughese shear zone (Fig. 2). This shear zone is a major line of weakness formed during the Ubendian Orogeny and reactivated by Recent rift faulting (Ray, 1974). It has localised extensional strain, which led to the development of the Ufipa Fault scarp as the southwestern border fault of the Rukwa Rift Basin as argued by Ring et al. (2002). These authors suggested that the Mughese shear zone controlled the position of the major strike direction of the western branch of the EARS during rifting. The influence of the Mughese shear zone in rift development have been demonstrated in the Nyasa (Malawi) Rift (Dawson et al., 2018; Laó-Dávila et al., 2015) south of the Rukwa Rift Basin.

In the southern part of Rukwa Rift Basin, the Mbeya Range fault zone, which is shown in detail in Figure 16, developed between the Lupa and Mbozi terranes of the Ubendian orogenic belt. This fault is parallel to the pre-existing greenschist-facies and retrograde sinistral strike-slip mylonitic structures flanking the shallow level of the Mesoproterozoic sedimentary rocks in the southern part of Rukwa Rift (Klerkx et al., 1998; Theunissen et al., 1996).

4.4 The extent of Chisi shear zone

The aeromagnetic data permit establishing for the first time that the Chisi shear zone (Fig. 3(a)), which pre-dates the Rukwa Rift Basin, continues from the northwest to the southeastern termination of the Basin (Fig. 17).

The Chisi shear zone is expressed as an escarpment at the land surface northwest of the Rukwa Rift Basin (Fig. 4) and its trace can been mapped through the Karema - Nkamba depression (in the vicinity of the towns of the same names; Fig. 4) as a WNW-ESE trending sinistral strike-slip mylonite ridge of the Karema-Chisi fault line (Fernandez-Alonso et al., 2001; Theunissen et al., 1996). It forms the boundary between the Ufipa terrane and Ubende terrane on the northwest of Rukwa Rift Basin and it is believed to mark the Pan-African suture between the Tanzanian Craton and Archaean – Paleoproterozoic Bangweulu cratonic block (Boniface and Schenk, 2012). This shear zone was formerly believed to provide a link with the NW striking Rukwa structures, including the Lupa Fault (Fernandez-Alonso et al., 2001), which is the border of the eastern margin of the Rukwa Rift Basin (Figs. 3 and 4). Within the Rukwa Rift Basin, the continuation of the Chisi shear zone is unclear, as it tends to disappear under the unconsolidated sediments of the basin (Fig. 3(a)).

The present results (e.g. Figs. 8 and 9), however, show a NW–SE single linear trending magnetic anomaly of ~150 km that marks the presence of the Chisi shear zone beneath the young Rukwa Lake sediments and, as such, it does not form a link with the Lupa Fault as was previously proposed (Fernandez-Alonso et al., 2001). This is shown in greater detail in Figure 17. The spatial extent and horizontal continuity of the shear zone and other prominent structures surrounding the Rukwa Rift Basin is shown in Figure. 17(b), which shows strong NW-SE trending structures delineated from magnetic anomalies. This shear zone, like other shear zones affecting the Rukwa Rift Basin, facilitated the localisation of extensional strain within the border faults of the Rukwa Rift Basin. It coincides with the Karema – Chisi fault line on the northwestern side of the Rukwa Rift Basin (Fig. 4 and 17(b)) and marks the Pan-African suture during the collision between the Tanzanian Craton and the Archaean-Paleoproteroic Bangweulu cratonic block. It also connects the Rukwa Rift Basin with the Lake Tanganyika Rift through the Karema – Nkamba depression in the northwestern side of Rukwa Rift Basin (Fig. 4).

5. Summary and Conclusions

The analysis of the SRTM DEM and aeromagnetic data highlights the significance role played by pre-existing Precambrian lithospheric (inasmuch as the upper crust is part of the lithosphere as a whole) structures on the development of continental rifts

The orientations of basement structures inferred from SRTM DEM and magnetic data are mainly trending NW-SE, which is consistent with the NW-trending Paleoproterozoic Ubendian orogenic belt. The border faults (the Lupa and Ufipa faults) generally follows (parallel) the pre-existing basement structures/foliation trends identified by alternating low and high magnetic anomalies. The Lupa and Livingstone faults, the latter being the NE bounding fault of the Nyasa (Malawi) lake segment of the western branch of the EARS, may be continuous beneath the cover of the intervening Rungwe Volcanic Province.

The orientation of pre-existing structures within the Paleoproterozoic terrains (including the Mughese and Chisi shear zones) facilitated the localisation of extensional strain within border faults that utilised the existence of inherited lithospheric heterogeneity (i.e., that the fossil lithospheric boundary between the Archaean and Proterozoic basement terranes was involved in the development of the Rukwa Rift Basin). Proterozoic mylonites constitute a source of shallow level mechanical anisotropy and define the general trend of the rift faults. These mylonites have been reactivated as complex multiphase rift faults or as normal and recent faults. The Paleoproterozoic NW trending Ubendian orogenic belt and its ductile lateral shear belt provided the deep level mechanical anisotropy and its reactivation, which is likely dextral oblique transtension,is considered as a leading mechanism of NW oriented Rukwa Rift Basin.

Acknowledgements

We acknowledge the financial support of BG Group Tanzania (now Shell) through the University of Dar es Salaam - University of Aberdeen - BG Tanzania (now Shell) Initiative. Tanzania Petroleum Development Corporation (TPDC) provided aeromagnetic data used in this study at no cost. We are grateful to the editors and anonymous reviewers for detailed and constructive reviews that improved the manuscript.

References

Aanyu, K., Koehn, D., 2011. Influence of pre-existing fabrics on fault kinematics and rift geometry of interacting segments: Analogue models based on the Albertine Rift (Uganda), Western Branch-East African Rift System. J. African Earth Sci. 59, 168–184. doi:10.1016/j.jafrearsci.2010.10.003

Abdelsalam, M.G., Atekwana, E.A., Keller, G.R., Klemperer, S.L., 2004. The Life Cycle of Continental Rifting as a Focus for U.S.-African scientific collaboration. Eos, Trans. Am. Geophys. Union 85, 22–23. doi:10.1029/2004EO470004

Anudu, G.K., Stephenson, R.A., Macdonald, D.I.M., 2014. Using high-resolution aeromagnetic data to recognise and map intra-sedimentary volcanic rocks and geological structures across the Cretaceous middle Benue Trough, Nigeria. J. African Earth Sci. 99, 625–636. doi:10.1016/j.jafrearsci.2014.02.017

Baranov, V., 1957. A new method for interpretation of aeromagnetic maps: pseudo-gravimetric anomalies. Geophysics 22, 359–382. doi:10.1190/1.1438369

Bastow, I.D., Keir, D., Daly, E., 2011. The Ethiopia Afar Geoscientific Lithospheric Experiment (EAGLE): Probing the transition from continental rifting to incipient seafloor spreading, in: Beccaluva, L., Bianchini, G., Wilson, M. (Eds.), Volcanism and Evolution of the African Lithosphere. Geological Society of America Special Paper 478, Boulder, Colorado, pp. 51–76. doi:10.1130/2011.2478(04)

Basu, N.K., Ikingura, J.R., 1984. Petrology of the marginal part of Mbozi syenite—gabbro complex, Mbozi District, Mbeya Region, Tanzania. J. African Earth Sci. 2, 155–160. doi:10.1016/S0731-7247(84)80010-5

Beyene, A., Abdelsalam, M.G., 2005. Tectonics of the Afar Depression: A review and synthesis. J. African Earth Sci. 41, 41–59.

doi:10.1016/j.jafrearsci.2005.03.003

Bialas, R.W., Buck, W.R., Qin, R., 2010. How much magma is required to rift a continent? Earth Planet. Sci. Lett. 292, 68–78. doi:10.1016/j.epsl.2010.01.021

Blakely, R.J., 1995. Potential Theory in Gravity and Magnetic Applications, Stanford-Cambridge Program. Cambridge University Press.

Blakely, R.J., Simpson, R.W., 1986. Approximating edges of source bodies from magnetic or gravity anomalies. Geophysics 51, 1494–1498. doi:10.1190/1.1442197

Boniface, N., Schenk, V., 2012. Neoproterozoic eclogites in the Paleoproterozoic Ubendian Belt of Tanzania: Evidence for a Pan-African suture between the Bangweulu Block and the Tanzania Craton. Precambrian Res. 208–211, 72–89. doi:10.1016/j.precamres.2012.03.014

Boniface, N., Schenk, V., Appel, P., 2014. Mesoproterozoic high-grade metamorphism in pelitic rocks of the northwestern Ubendian Belt: Implication for the extension of the Kibaran intra-continental basins to Tanzania. Precambrian Res. 249, 215–228. doi:10.1016/j.precamres.2014.05.010

Boniface, N., Schenk, V., Appel, P., 2012. Paleoproterozoic eclogites of MORB-type chemistry and three Proterozoic orogenic cycles in the Ubendian Belt (Tanzania): Evidence from monazite and zircon geochronology, and geochemistry. Precambrian Res. 192–195, 16–33. doi:10.1016/j.precamres.2011.10.007

Bridges, D.L., Mickus, K.L., Gao, S.S., Abdelsalam, M.G., Alemu, A., 2012. Magnetic stripes of a transitional continental rift in Afar. Geology 40, 203–206. doi:10.1130/G32697.1

Briggs, I.C., 1974. Machine Contouring Using Minimum Curvature. Geophysics 39, 39. doi:10.1190/1.1440410

Brock, P.W.G., 1961. Geology of the Mbozi syenite-gabbro complex. QDS 257. Dodoma, Tanzania.

Buck, W.R., 2006. The role of magma in the development of the Afro-Arabian Rift System. Geol. Soc. London, Spec. Publ. 259, 43–54. doi:10.1144/GSL.SP.2006.259.01.05

Calais, E., D'Oreye, N., Albaric, J., Deschamps, A., Delvaux, D., Déverchère, J., Ebinger, C.J., Ferdinand, R.W., Kervyn, F., Macheyeki, A.S., Oyen, A., Perrot, J., Saria, E., Smets, B., Stamps, D.S., Wauthier, C., 2008. Strain accommodation by slow slip and dyking in a youthful continental rift, East Africa. Nature 456, 783–787. doi:10.1038/nature07478

Chorowicz, J., 2005. The East African rift system. J. African Earth Sci. 43, 379–410. doi:10.1016/j.jafrearsci.2005.07.019

Cordell, L., Grauch, V.J.S., 1985. Mapping Basement Magnetization Zones from Aeromagnetic Data in the San Juan Basin, New Mexico, in: Hinze, W.J. (Ed.), The Utility of Regional Gravity and Magnetic Anomaly Maps. SEG, pp. 181–197. doi:10.1190/1.0931830346.ch16

Daly, M.C., 1988. Crustal shear zones in central africa: A kinematic approach to proterozoic tectonics. Episodes 11, 5–11.

Daly, M.C., Chorowicz, J., Fairhead, J.D., 1989. Rift basin evolution in Africa: the influence of reactivated steep basement shear zones. Geol. Soc. London, Spec. Publ. 44, 309–334. doi:10.1144/GSL.SP.1989.044.01.17

Dawson, S.M., Laó-Dávila, D.A., Atekwana, E.A., Abdelsalam, M.G., 2018. The influence of the Precambrian Mughese Shear Zone structures on strain accommodation in the northern Malawi Rift. Tectonophysics 722, 53–68. doi:10.1016/j.tecto.2017.10.010

Delvaux, D., Fronhoffs, A., Hus, R., 1999. Normal fault splays, relay ramps and transfer zones in the central part of the baikal rift basin: Insight from digital topography and bathymetry. Bull. des Centres Rech. Explor. Prod. ELF aquitaine 22, 341–358.

Delvaux, D., Hanon, M., 1993. Neotectonics of the Mbeya Area, Sw Tanzania. Mus. roy. Afr. centr. 97, 87–97.

Delvaux, D., Kervyn, F., Macheyeki, A.S., Temu, E.B., 2012. Geodynamic significance of the TRM segment in the East African Rift (W-Tanzania): Active tectonics and paleostress in the Ufipa plateau and Rukwa basin. J. Struct. Geol. 37, 161–180. doi:10.1016/j.jsg.2012.01.008

Delvaux, D., Kervyn, F., Vittori, E., Kajara, R.S.A., Kilembe, E.A., 1998. Late Quaternary tectonic activity and lake level change in the Rukwa Rift Basin. J. African Earth Sci. 26, 397–421. doi:10.1016/S0899-5362(98)00023-2

Dentith, M.C., 2011. Magnetic Methods, Airborne, in: Gupta, H.K. (Ed.), Encyclopedia of Solid Earth Geophysics SE - 119, Encyclopedia of Earth Sciences Series. Springer Netherlands, pp. 761–766. doi:10.1007/978-90-481-

8702-7_119

Dypvik, H., Nesteby, H., Ruden, F., Aagaard, P., Johansson, T., Msindai, J., Massay, C., 1990. Upper Paleozoic and Mesozoic sedimentation in the Rukwa-Tukuyu Region, Tanzania. J. African Earth Sci. 11, 437–456. doi:10.1016/0899-5362(90)90022-7

Ebinger, C.J., 1989a. Geometric and kinematic development of border faults and accommodation zones, Kivu-Rusizi Rift, Africa. Tectonics 8, 117–133.

Ebinger, C.J., 1989b. Tectonic development of the western branch of the East African rift system. GSA Bull. 101, 885–903. doi:10.1130/0016-7606(1989)101<0885

Ebinger, C.J., Casey, M., 2001. Continental breakup in magmatic provinces: An Ethiopian example. Geology 29, 527–530. doi:10.1130/0091-7613(2001)029<0527:CBIMPA>2.0.CO;2

Ebinger, C.J., Deino, A.L., Drake, R.E., Tesha, A.L., 1989. Chronology of volcanism and rift basin propagation: Rungwe Volcanic Province, East Africa. J. Geophys. Res. Solid Earth 94, 15785–15803. doi:10.1029/JB094iB11p15785

Ebinger, C.J., Rosendahl, B.R., Reynolds, D.J., 1987. Tectonic model of the Malawi rift, Africa. Tectonophysics 141, 215–235. doi:10.1016/0040-1951(87)90187-9

Fairhead, J.D., Salem, A., Cascone, L., Hammill, M., Masterton, S., Samson, E., 2011. New developments of the magnetic tilt-depth method to improve structural mapping of sedimentary basins. Geophys. Prospect. 59, 1072–

1086. doi:10.1111/j.1365-2478.2011.01001.x

Farr, T.G., Rosen, P.A., Caro, E., Crippen, R., Duren, R., Hensley, S., Kobrick, M., Paller, M., Rodriguez, E., Roth, L., Seal, D., Shaffer, S., Shimada, J., Umland, J., Werner, M., Oskin, M., Burbank, D., Alsdorf, D., 2007. The shuttle radar topography mission. Rev. Geophys. 45, 1–33. doi:10.1029/2005RG000183.1

Fernandez-Alonso, M., Delvaux, D., Klerkx, J., Theunissen, K., 2001. Structural link between Tanganyika-and Rukwa-rift basins at Karema-Nkamba (Tanzania): Basement structural control and recent evolution. Mus. Roy. Afr. Centr. tervuren (Belg.), Dépt. Géol. Min. Rapp. Ann. 1999–2000, 91–100.

Flannery, J.W., Rosendahl, B.R., 1990. The seismic stratigraphy of Lake Malawi, Africa: implications for interpreting geological processes in lacustrine rifts. J. African Earth Sci. 10, 519–548. doi:10.1016/0899-5362(90)90104-M

Fontijn, K., Delvaux, D., Ernst, G.G.J., Kervyn, M., Mbede, E.I., Jacobs, P., 2010. Tectonic control over active volcanism at a range of scales: Case of the Rungwe Volcanic Province, SW Tanzania; and hazard implications. J. African Earth Sci. 58, 764–777. doi:10.1016/j.jafrearsci.2009.11.011

Fraser, S.I., Fraser, A.J., Lentini, M.R., Gawthorpe, R.L., 2007. Return to rifts - the next wave: fresh insights into the petroleum geology of global rift basins. Pet. Geosci. 13, 99–104. doi:10.1144/1354-079307-749

Fritz, H., Abdelsalam, M.G., Ali, K.A., Bingen, B., Collins, A.S., Fowler, A.R., Ghebreab, W., Hauzenberger, C.A., Johnson, P.R., Kusky, T.M., Macey, P., Muhongo, S.M., Stern, R.J., Viola, G., 2013. Orogen styles in the East African Orogen: A review of the Neoproterozoic to Cambrian tectonic evolution. J. African Earth Sci. 86, 65–106. doi:10.1016/j.jafrearsci.2013.06.004

Geosoft Inc., 2011. MAGMAP Filtering Tutorial.

Harper, R.M., Stone, D.M., Morley, C.K., 1999. Geophysics of the Usangu Flats, Tanzania, in: Morley, C.K. (Ed.), Geoscience of Rift Systems - Evolution of East Africa. AAPG Studies in Geology, pp. 111–114.

Heron, P.J., Pysklywec, R.N., Stephenson, R.A., 2016. Lasting mantle scars lead to perennial plate tectonics. Nat. Commun. 7, 1–7. doi:10.1038/ncomms11834

Holdsworth, R.E., Stewart, M., Imber, J., Strachan, R.A., 2001. The structure and rheological evolution of reactivated continental fault zones: a review and case study. Geol. Soc. London, Spec. Publ. 184, 115–137. doi:10.1144/gsl.sp.2001.184.01.07

Jacobsen, B.H., 1987. A case for upward continuation as a standard separation filter for potential-field maps. Geophysics 52, 1138–1148. doi:10.1190/1.1442378

Jenness, J., 2014. Polar plots for ArcGIS. Jenness Enterp.

Jenness, J., 2013. DEM Surface Tools: Extension for ArcGIS.

Kabete, J.M., McNaughton, N.J., Groves, D.I., Mruma, A.H., 2012. Reconnaissance SHRIMP U-Pb zircon geochronology of the Tanzania

Craton: Evidence for Neoarchean granitoid-greenstone belts in the Central Tanzania Region and the Southern East African Orogen. Precambrian Res. 216–219, 232–266. doi:10.1016/j.precamres.2012.06.020

Kampunzu, A.B., Bonhomme, M.G., Kanika, M., 1998. Geochronology of volcanic rocks and evolution of the Cenozoic western branch of the East African Rift system. J. African Earth Sci. 26, 441–461. doi:10.1016/S0899-5362(98)00025-6

Katumwehe, A.B., Abdelsalam, M.G., Atekwana, E.A., 2015. The role of pre-existing Precambrian structures in rift evolution: The Albertine and Rhino grabens, Uganda. Tectonophysics 646, 117–129. doi:10.1016/j.tecto.2015.01.022

Kazimoto, E.O., Schenk, V., Appel, P., 2015. Granulite-facies metamorphic events in the northwestern Ubendian Belt of Tanzania: Implications for the Neoarchean to Paleoproterozoic crustal evolution. Precambrian Res. 256, 31–47. doi:10.1016/j.precamres.2014.10.016

Kazimoto, E.O., Schenk, V., Berndt, J., 2014. Neoarchean and Paleoproterozoic crust formation in the Ubendian Belt of Tanzania: Insights from zircon geochronology and geochemistry. Precambrian Res. 252, 119–144. doi:10.1016/j.precamres.2014.06.020

Kervyn, F., Ayub, S., Kajara, R.S.A., Kanza, E., Temu, E.B., 2006. Evidence of recent faulting in the Rukwa rift (West Tanzania) based on radar interferometric DEMs. J. African Earth Sci. 44, 151–168. doi:10.1016/j.jafrearsci.2005.10.008

Kilembe, E.A., Rosendahl, B.R., 1992. Structure and stratigraphy of the Rukwa rift. Tectonophysics 209, 143–158. doi:10.1016/0040-1951(92)90016-Y

Kinabo, B.D., Atekwana, E.A., Hogan, J.P., Modisi, M.P., Wheaton, D.D., Kampunzu, A.B., 2007. Early structural development of the Okavango rift zone, NW Botswana. J. African Earth Sci. 48, 125–136. doi:10.1016/j.jafrearsci.2007.02.005

Klerkx, J., Theunissen, K., Delvaux, D., 1998. Persistent fault controlled basin formation since the Proterozoic along the Western Branch of the East African Rift. J. African Earth Sci. 26, 347–361. doi:10.1016/S0899-5362(98)00020-7

Kolawole, F., Atekwana, E.A., Laó-Dávila, D.A., Abdelsalam, M.G., Chindandali, P.R.N., Salima, J., Kalindekafe, L., 2018. Active deformation of Malawi Rift's North Basin hinge zone modulated by reactivation of pre-existing Precambrian shear zone fabric. Tectonics 37, 1–22. doi:10.1002/2017TC004628

Kolawole, F., Atekwana, E.A., Malloy, S., Stamps, D.S., Grandin, R., Abdelsalam, M.G., Leseane, K., Shemang, E.M., 2017. Aeromagnetic, gravity, and Differential Interferometric Synthetic Aperture Radar analyses reveal the causative fault of the 3 April 2017 Mw6.5 Moiyabana, Botswana, earthquake. Geophys. Res. Lett. 44, 8837–8846. doi:10.1002/2017GL074620

Korme, T., Acocella, V., Abebe, B., 2004. The Role of Pre-existing Structures in the Origin, Propagation and Architecture of Faults in the Main Ethiopian

Rift. Gondwana Res. 7, 467–479. doi:10.1016/S1342-937X(05)70798-X

Kumanan, C.J., Saravanavel, J., Palanivel, K., 2011. Virtues of 3D GIS in Mapping Earth-Subsurfaces Geological System/Process, in: 12th ESRI India User Conference. ESRI India.

Laó-Dávila, D.A., Al-Salmi, H.S., Abdelsalam, M.G., Atekwana, E.A., 2015. Hierarchical segmentation of the Malawi Rift: The influence of inherited lithospheric heterogeneity and kinematics in the evolution of continental rifts. Tectonics 34, 2399–2417. doi:10.1002/2015TC003953

Lawley, C.J.M., Selby, D., Condon, D.J., Horstwood, M.S.A., Millar, I., Crowley, Q., Imber, J., 2013. Lithogeochemistry, geochronology and geodynamic setting of the Lupa Terrane, Tanzania: Implications for the extent of the Archean Tanzanian Craton. Precambrian Res. 231, 174–193. doi:10.1016/j.precamres.2013.02.012

Le Gall, B., Gernigon, L., Rolet, J., Ebinger, C.J., Gloaguen, R., Nilsen, O., Dypvik, H., Deffontaines, B., Mruma, A.H., 2004. Neogene-Holocene rift propagation in central Tanzania: Morphostructural and aeromagnetic evidence from the Kilombero area. Bull. Geol. Soc. Am. 116, 490–510. doi:10.1130/B25202.1

Lenoir, J.L., Liégeois, J.P., Theunissen, K., Klerkx, J., 1994. The Palaeoproterozoic Ubendian shear belt in Tanzania: geochronology and structure. J. African Earth Sci. 19, 169–184. doi:10.1016/0899-5362(94)90059-0

Leseane, K., Atekwana, E.A., Mickus, K.L., Abdelsalam, M.G., Shemang, E.M., Atekwana, E.A., 2015. Thermal perturbations beneath the incipient Okavango Rift Zone, northwest Botswana. J. Geophys. Res. Solid Earth 120, 1210–1228. doi:10.1002/2014JB011029.

Manya, S., 2014. Geochemistry of the Palaeoproterozoic gabbros and granodiorites of the Saza area in the Lupa Goldfield, southwestern Tanzania. J. African Earth Sci. 100, 401–408. doi:10.1016/j.jafrearsci.2014.07.016

Mark, R.K., 1992. A multidirectional, oblique-weighted, shaded-relief image of the Island of Hawaii, Open-File Report.

Marobhe, I., 1989. Interpretation of aerogeophysical anomalies of Southwestern Tanzania, Bulletin (Geologian tutkimuskeskus (Finland)). Geologian Tutkimuskeskus.

Mbede, E.I., 1993. Tectonic Development of the Rukwa Rift Basin in SW Tanzania. Fachber. Geowiss., TU Berlin.

McConnell, R.B., 1950. Outline of the geology of Ufipa and Ubende. Geological Survey Dept., Dodoma, Tanganyika Territory.

McConnell, R.B., 1972. Geological Development of the Rift System of Eastern Africa. Geol. Soc. Am. Bull. 83, 2549–2572. doi:10.1130/0016-7606(1972)83[2549:GDOTRS]2.0.CO;2

McConnell, R.B., 1980. A resurgent taphrogenic lineament of Precambrian origin in eastern Africa. J. Geol. Soc. London 137, 483–489. doi:10.1144/gsjgs.137.4.0483

ACCEPTED MANUSCRIPT

Miller, H.G., Singh, V., 1994. Potential field tilt—a new concept for location of potential field sources. J. Appl. Geophys. 32, 213–217. doi:10.1016/0926-9851(94)90022-1

Misra, A.A., Mukherjee, S., 2015. Tectonic Inheritance in Continental Rifts and Passive Margins. Springer International Publishing.

Mnali, S., 1999. Palaeoproterozoic Felsic Magmatism and Associated Gold-Quartz Vein Mineralization in Western Part of the Lupa Gold Field, South-Western Tanzania. University of Dar es Salaam.

Morley, C.K., 1999. How successful are analogue models in addressing the influence of pre-existing fabrics on rift structure? J. Struct. Geol. 21, 1267–1274. doi:10.1016/S0191-8141(99)00075-9

Morley, C.K., Cunningham, S.M., Wescott, W.A., Harper, R.M., 1999. The geology and Geophysics of the Rukwa Rift, in: Morley, C.K. (Ed.), Geoscience of Rift Systems - Evolution of East Africa. AAPG Studies in Geology, pp. 91–110.

Morley, C.K., Vanhauwaert, P., De Batist, M., 2000. Evidence for high-frequency cyclic fault activity from high-resolution seismic reflection survey, Rukwa Rift, Tanzania. J. Geol. Soc. London. 157, 983–994. doi:10.1144/jgs.157.5.983

Mshiu, E.E., Gläßer, C., Borg, G., 2015. Identification of hydrothermal paleofluid pathways, the pathfinders in the exploration of mineral deposits: A case study from the Sukumaland Greenstone Belt, Lake Victoria Gold Field, Tanzania. Adv. Sp. Res. 55, 1117–1133.

doi:10.1016/j.asr.2014.11.024

Muhongo, S.M., Tuisku, P., Mnali, S., Temu, E.B., Appel, P., Stendal, H., 2002. High-pressure granulite-facies metagabbros in the Ubendian Belt of SW Tanzania: preliminary petrography and P–T estimates. J. African Earth Sci. 34, 279–285.

Mulibo, G.D., Nyblade, A.A., 2016. The seismotectonics of Southeastern Tanzania: Implications for the propagation of the eastern branch of the East African Rift. Tectonophysics 674, 20–30. doi:10.1016/j.tecto.2016.02.009

Peirce, J.W., Lipkov, L., 1988. Structural interpretation of the Rukwa Rift, Tanzania. Geophysics 53, 824–836. doi:10.1190/1.1442517

Phillips, J.D., 2002. Processing and interpretation of aeromagnetic data for the Santa Cruz Basin - Patagonia Mountains area, south-central Arizona, USGS Open-File Report -02-98. Reston, VA.

Phillips, J.D., 2001. Designing matched bandpass and azimuthal filters for the separation of potential-field anomalies by source region and source type, in: ASEG 15th Geophysical Conference and Exhibition, August 2001, Brisbane.

Phillips, J.D., Hansen, R.O., Blakely, R.J., 2007. The use of curvature in potential-field interpretation. Explor. Geophys. 38, 111–119. doi:10.1071/EG07014

Ramli, M.F., Yusof, N., Yusoff, M.K., Juahir, H., Shafri, H.Z.M., 2010. Lineament mapping and its application in landslide hazard assessment: a review. Bull. Eng. Geol. Environ. 69, 215–233. doi:10.1007/s10064-009-0255-5

Ray, G.E., 1974. The structural and metamorphic geology of northern Malawi. J. Geol. Soc. London. 130, 427–440. doi:10.1144/gsjgs.130.5.0427

Reed, C.A., Almadani, S., Gao, S.S., Elsheikh, A.A., Cherie, S., Abdelsalam, M.G., Thurmond, A.K., Liu, K.H., 2014. Receiver function constraints on crustal seismic velocities and partial melting beneath the Red Sea rift and adjacent regions, Afar Depression. J. Geophys. Res. Solid Earth 119, 2138–2152. doi:10.1002/2013JB010719

Ring, U., 1994. The influence of preexisting structure on the evolution of the Cenozoic Malawi rift (East African rift system). Tectonics 13, 313–326.

Ring, U., Betzler, C., 1995. Geology of the Malawi Rift: kinematic and tectonosedimentary background to the Chiwondo Beds, northern Malawi. J. Hum. Evol. doi:10.1006/jhev.1995.1003

Ring, U., Kröner, A., Buchwaldt, R., Toulkeridis, T., Layer, P.W., 2002. Shear-zone patterns and eclogite-facies metamorphism in the Mozambique belt of northern Malawi, east-central Africa: Implications for the assembly of Gondwana. Precambrian Res. 116, 19–56. doi:10.1016/S0301-9268(01)00233-9

Ring, U., Schwartz, H.L., Bromage, T.G., Sanaane, C., 2005. Kinematic and sedimentological evolution of the Manyara Rift in northern Tanzania, East Africa. Geol. Mag. 142, 355. doi:10.1017/S0016756805000841

Roberts, E.M., O’Connor, P.M., Gottfried, M.D., Stevens, N.J., Kapilima, S., Ngasala, S., 2004. Revised stratigraphy and age of the Red Sandstone Group in the Rukwa Rift Basin, Tanzania. Cretac. Res. 25, 749–759.

doi:10.1016/j.cretres.2004.06.007

Roberts, E.M., O'Connor, P.M., Stevens, N.J., Gottfried, M.D., Jinnah, Z.A., Ngasala, S., Choh, A.M., Armstrong, R.A., 2010. Sedimentology and depositional environments of the Red Sandstone Group, Rukwa Rift Basin, southwestern Tanzania: New insight into Cretaceous and Paleogene terrestrial ecosystems and tectonics in sub-equatorial Africa. J. African Earth Sci. 57, 179–212. doi:10.1016/j.jafrearsci.2009.09.002

Roberts, E.M., Stevens, N.J., O'Connor, P.M., Dirks, P.H.G.M., Gottfried, M.D., Clyde, W.C., Armstrong, R.A., Kemp, A.I.S., Hemming, S.R., 2012. Initiation of the western branch of the East African Rift coeval with the eastern branch. Nat. Geosci. 5, 289–294. doi:10.1038/ngeo1432

Rosendahl, B.R., 1987. Architecture of Continental Rifts with Special Reference to East Africa. Ann. Rev. Earth Planet Sci. 15, 445–503.

Saalmann, K., Mänttäri, I., Nyakecho, C., Isabirye, E., 2016. Age, tectonic evolution and origin of the Aswa Shear Zone in Uganda: Activation of an oblique ramp during convergence in the East African Orogen. J. African Earth Sci. 117, 303–330. doi:10.1016/j.jafrearsci.2016.02.002

Schmeling, H., 2010. Dynamic models of continental rifting with melt generation. Tectonophysics 480, 33–47. doi:10.1016/j.tecto.2009.09.005

Şengör, A.M.C., 2011. Continental rifts, in: Gupta, H.K. (Ed.), Encyclopedia of Solid Earth Geophysics. Springer Netherlands, Dordrecht, pp. 40–55.

Simiyu, S.M., Keller, G.R., 2001. An integrated geophysical analysis of the upper crust of the southern Kenya rift. Geophys. J. Int. 147, 543–561.

doi:10.1046/j.0956-540x.2001.01542.x

Smets, B., Delvaux, D., Ross, K.A., Poppe, S., Kervyn, M., D'Oreye, N., Kervyn, F., 2016. The role of inherited crustal structures and magmatism in the development of rift segments: Insights from the Kivu basin, western branch of the East African Rift. Tectonophysics 683, 62–76. doi:10.1016/j.tecto.2016.06.022

Smets, B., Kervyn, M., d'Oreye, N., Kervyn, F., 2015. Spatio-temporal dynamics of eruptions in a youthful extensional setting: Insights from Nyamulagira Volcano (D.R. Congo), in the western branch of the East African Rift. Earth-Science Rev. 150, 305–328. doi:10.1016/j.earscirev.2015.08.008

Smith, M.J., Clark, C.D., 2005. Methods for the visualization of digital elevation models for landform mapping. Earth Surf. Process. Landforms 30, 885–900. doi:10.1002/esp.1210

Stendal, H., Frei, R., Muhongo, S.M., Rasmussen, T.M., Mnali, S., Petro, F., Temu, E.B., 2004. Gold potential of the Mpanda Mineral Field, SW Tanzania: evaluation based on geological, lead isotopic and aeromagnetic data. J. African Earth Sci. 38, 437–447. doi:10.1016/j.jafrearsci.2004.04.005

Sutton, J., Watson, J.V., 1986. Architecture of the continental lithosphere. Philos. Trans. R. Soc. London. A317, 5–12.

Swain, C.J., 1976. A FORTRAN IV program for interpolating irregularly spaced data using the difference equations for minimum curvature. Comput. Geosci. 1, 231–240. doi:10.1016/0098-3004(76)90071-6

Theunissen, K., Klerkx, J., Melnikov, A., Mruma, A.H., 1996. Mechanisms of inheritance of rift faulting in the western branch of the East African Rift, Tanzania. Tectonics 15, 776–790. doi:10.1029/95TC03685

Thomas, R.J., Spencer, C., Bushi, A.M., Baglow, N., Boniface, N., de Kock, G., Horstwood, M.S.A., Hollick, L., Jacobs, J., Kajara, R.S.A., Kamihanda, G., Key, R.M., Maganga, Z., Mbawala, F., McCourt, W., Momburi, P., Moses, F., Mruma, A.H., Myambilwa, Y., Roberts, N.M.W., Saidi, H., Nyanda, P., Nyoka, K., Millar, I., 2016. Geochronology of the central Tanzania Craton and its southern and eastern orogenic margins. Precambrian Res. 277, 47–67. doi:10.1016/j.precamres.2016.02.008

Tiercelin, J.J., Chorowicz, J., Bellon, H., Richert, J.P., Mwanbene, J.T., Walgenwitz, F., 1988. East African rift system: offset, age and tectonic significance of the Tanganyika-Rukwa-Malawi intracontinental transcurrent fault zone. Tectonophysics 148, 241–252. doi:http://dx.doi.org/10.1016/0040-1951(88)90133-3

van der Beek, P., Mbede, E.I., Andriessen, P., Delvaux, D., 1998. Denudation history of the Malawi and Rukwa Rift flanks (East African Rift system) from apatite fission track thermochronology. J. African Earth Sci. 26, 363–385. doi:10.1016/S0899-5362(98)00021-9

Verduzco, B., Fairhead, J.D., Green, C.M., Mackenzie, C., 2004. New insights into magnetic derivatives for structural mapping. Lead. Edge 23, 116–119. doi:10.1190/1.1651454

Vittori, E., Delvaux, D., Kervyn, F., 1997. Kanda fault: A major seismogenic element west of the Rukwa Rift (Tanzania, East Africa). J. Geodyn. 24, 139–

153. doi:10.1016/S0264-3707(96)00038-5

Wood, D.A., Zal, H.J., Scholz, C.A., Ebinger, C.J., Nizere, I., 2017. Evolution of the Kivu Rift, East Africa: interplay among tectonics, sedimentation and magmatism. Basin Res. 29, 175–188. doi:10.1111/bre.12143

Wright, T.J., Ebinger, C.J., Biggs, J., Ayele, A., Yirgu, G., Keir, D., Stork, A., 2006. Magma-maintained rift segmentation at continental rupture in the 2005 Afar dyking episode. Nature 442, 291–294. doi:10.1038/nature04978

Figure Captions

Figure 1: The eastern and western branches of East African Rift System showing main rift fault escarpments mapped from SRTM DEM (NASA). ASZ = Aswa Shear Zone; EYR = Eyasi Rift; KR = Kenya Rift; LA = Lake Albert; LT = Lake Tanganyika; LTU = Lake Turkana; LN = Lake Nyasa/Malawi; LR = Lake Rukwa; LV = Lake Victoria; MER = Main Ethiopian Rift; MNR = Manyara Rift; PNR = Pangani Rift. The location of Figure2 is shown with the blue dashed rectangle.

Figure 2. Tectonic map of the Eastern and Western Branches of the East African Rift System (EARS) modified from Katumwehe et al. (2015). ALG = Albertine graben; LA = Lake Albert; LE= Lake Edward; LK = Lake Kivu; LM = Lake Malawi (Nyasa); LN = Lake Natron; LR = Lake Rukwa; LT = Lake Tanganyika; LTU = Lake Turkana; MSZ = Mughese shear zone; RHG = Rhino graben. The position of the Mughese shear zone is modified from Fritz et al. (2013). The volcanic fields are Bukavu (B), Mwenga Kamitunga (MK), Rungwe

Volcanic Province (RVP), Toro Ankole (TA), and Virunga (V). The white dashed rectangle is location of the study area (Fig. 3).

Figure 3: a) Simplified geological map of the Rukwa Rift Basin showing major tectonic features. KA = Katuma terrane; LU = Lupa terrane; MB = Mbozi Terrane; MST = Msongano trough; SNT = Songwe trough; RVP = Rungwe Volcanic Province; UB = Ubende terrane; UF= Ufipa terrane; UP = Upangwa terrane; USB = Usangu Basin; WA = Wakole terrane. Blue line labelled A-B shows the area of the cross-section drawn in (b). b) A generalised geological cross-section across the Rukwa Rift Basin. KALF = Kalambo Fault; KF = Kanda Fault; LF = Lupa Fault; UF = Ufipa Fault.

Figure 4: Shuttle Radar Topography Mission Digital Elevation Model (SRTM DEM) of the study area extracted from USGS website http://earthexplorer.usgs.gov/ superimposed with known geological structures/faults (black lines). The dashed white rectangle indicate the area shown in Figure 5. The dashed red line indicates the Karema – Chisi fault line extension based on the interpretation by Fernandez-Alonso et al. (2001). White lines indicate the border faults of the Rukwa Rift Basin. KA = Karema town; NK = Nkamba town; RVP = Rungwe Volcanic Province.

Figure 5: Types of images derived from topographic data used in this study. a) colour-shaded elevation image, b) colour scaled slope image derived from elevation data, c) Multidirectional Oblique Weighted (MDOW) hillshade image and d) combination of images illustrated from (a) to (c) using transparency option superimposed with the extracted lineaments (black lines). Ornamented white lines indicate the border faults of the Rukwa Rift Basin. See Figure 4 for location.

Figure 6: a) Radially symmetric power spectrum of the study area (green) and the power spectrum of a matching four-layer equivalent model (blue). b) The matched bandpass filters corresponding to the four equivalent layers. c) Filtered Reduced to Pole total magnetic anomaly map of the study area. This figure was obtained after matched bandpass filter of cut-off wavelength of about 7000 m was applied to TMI grid to emphasise deeper magnetic anomaly sources (longer wavelength anomalies > 6.42 km), which is believed to be caused by the basement rocks of the Paleoproterozoic Ubendian orogenic belt underlying the Rukwa Rift Basin. The white lines are the known major tectonic features (faults/structures).

Figure 7: Total horizontal derivative of the filtered Reduced to Pole total magnetic intensity anomaly map of the study area. The letters A-E are the magnetic domains of the study area indicated by black rectangles and are – discussed later. RRB = Rukwa Rift Basin; RVP = Rungwe Volcanic Province.

Figure 8: Tilt derivative map derived from the ratio of the vertical and horizontal derivatives of the filtered Reduced to Pole total magnetic intensity anomaly map overlain with major tectonic features (faults/lineaments) within the study area. It greatly enhances, delineates and map both shallow and relatively deep causative geological and/or tectonic features. The maxima on this map define the extent and edges of the causative features across the area. The dashed rectangle indicate the area shown in Figure 17

Figure 9: Positive Tilt derivative map of the study area extracted from tilt derivative map shown in Figure 8 using Grid Math Builder from Oasis Montaj software. This image shows the spatial and lateral extent of the magnetic

anomalies of the study area. Note the clear spatial extent and lateral continuity of the Chisi shear zone and other prominent magnetic anomalies that are highlighted in this figure.

Figure 10: a) Structural map of the study area generated from the extraction of Precambrian fabrics/structures from edge detection filters of aeromagnetic data in black line segments and interpretation of Shuttle Radar Topography Mission (SRTM) Digital Elevation Model (DEM) in unadorned red line segments. RVP = Rungwe Volcanic Province. b) Rose diagram showing the trends of lineaments extracted from aeromagnetic data. c) Rose diagram showing the trends of basement fabrics/lineaments extracted from SRTM DEM data.

Figure 11: a) Multidirectional Oblique Weighted (MDOW) hillshade image of domain A (located in Fig. 7). Red lines indicate the traces of pre-existing Precambrian structures/lineaments extracted from the SRTM DEM data. b) The total horizontal derivative map of the filtered Reduced to Pole total intensity anomaly map of domain A. This domain corresponds to part of the Tanzanian Craton consisting of orthogneissic rocks. c) Structural interpretation map of the domain A showing pre-existing Precambrian structural trends/fabrics extracted from the edge detection techniques. d) Rose diagram showing the orientation of the pre-existing Precambrian structural trends/fabrics extracted from magnetic data using semi-automatic edge detection techniques. The N-S trending magnetic fabrics are predominant in this figure with minor NW-SE trending magnetic fabrics.

Figure 12: a) Multidirectional Oblique Weighted (MDOW) hillshade image of domain B (located in Fig. 7). Red lines indicate the traces of pre-existing

Precambrian structures/lineaments extracted from the SRTM DEM data. b) The total horizontal derivative map of the filtered Reduced to Pole total intensity anomaly map of domain B. c) Structural interpretation map of the domain B showing pre-existing Precambrian structural trends/fabrics extracted from the edge detection techniques. d) Rose diagram showing the orientation of the pre-existing Precambrian structures/fabrics extracted from magnetic data using semi-automatic edge detection techniques. This figure show that the NW-SE trending magnetic fabrics are dominant with minor N-S trending magnetic fabrics. Note that the dashed white lines in a) and b) as well as the dashed red lines in c) represent the boundaries of the Katuma, Wakole, Ubende and part of the Ufipa terranes.

Figure 13: a) Multidirectional Oblique Weighted (MDOW) hillshade image of domain C (located in Fig. 7). Red lines indicate the traces of pre-existing Precambrian structures/lineaments extracted from the SRTM DEM data. b) The total horizontal derivative map of the filtered Reduced to Pole total intensity anomaly map of domain C. c) Structural interpretation map of the domain C showing pre-existing Precambrian structural trends/fabrics extracted from the edge detection techniques. d) Rose diagram showing the orientation of the pre-existing Precambrian structures/fabrics extracted from magnetic data using semi-automatic edge detection techniques. In this figure there is no definite orientation of structures mapped from magnetic data.

Figure 14: a) Multidirectional Oblique Weighted (MDOW) hillshade image of domain D (located in Fig. 7). This domain represents part of the Ufipa terrane which is one of the terranes constituting the Paleoproterozic Ubendian orogenic

belt. Red lines indicate the traces of pre-existing Precambrian structures/lineaments extracted from the SRTM DEM data. b) The total horizontal derivative of the filtered Reduced to Pole total magnetic intensity anomaly map of domain D. c) Structural interpretation map of the domain D showing pre-existing Precambrian structural trends extracted from the edge detection techniques. Red lines represent rift border faults extracted from the Shuttle Radar Topography Mission (SRTM) Digital Elevation Model (DEM) data shown in Fig. 4. Comparison of the structures extracted from magnetic data and the structures mapped form SRTM DEM indicates a close parallelism between the northestern and southwestern border fault of the Rukwa Rift Basin. d) Rose diagram showing the orientation of the pre-existing Precambrian structures extracted from magnetic data using semi-automatic edge detection techniques. The strike orientation of the extracted structures from magnetic data in this domain is strongly oriented in a strike of 330º.

Figure 15: a) Multidirectional Oblique Weighted (MDOW) hillshade image of domain E (located in Fig. 7). Red lines indicates traces of the pre-existing Precambrian structural fabric and rift border faults which were extracted from the interpretation of the SRTM DEM data. b) The total horizotal derivative of the filtered Reduced to Pole total magnetic intensity anomaly map of domain E. Magnetic anomalies in this domain corresponds to rocks of the Mbozi terrane which is one of the terranes forming the Paleoproterozoic Ubendian orogenic belt. RVP = Rungwe Volcanic Province. c) Structural interpretation map of domain E showing pre-existing Precambrian structural trends extracted from the edge detection techniques. d) Rose diagram showing the orientation of the pre-existing Precambrian structures extracted from magnetic data using semi-

automatic edge detection techniques. The strike orientation of these structures are dominant in a NW-SE direction with minor N-S trends.

Figure 16: Shuttle Radar Topography Mission (SRTM) Digital Elevation Model (DEM) of the southern part of the Rukwa Rift Basin showing the extent of the Mbeya Range Fault and other prominent pre-existing Precambrian faults. Traces of the pre-existing Precambrian structural fabric and rift border faults are extracted from the interpretation of the SRTM DEM data.

Figure 17: a) Tilt derivative image of the NW Rukwa Rift Basin derived from the ratio of the vertical and Total Horizontal Derivatives of the filtered reduced to pole total magnetic intensity showing the extent of the Chisi shear zone. The black dashed line indicate the Karema – Chisi fault extension based on the interpretation by Fernandez-Alonso et al. (2001). b) Structural interpretation of the NW Rukwa Rift Basin extracted from aeromagnetic data showing the spatial extent and lateral continuity of the Chisi shear zone and other prominent structures surrounding the Rukwa Rift Basin. Rift border faults are extracted from SRTM DEM data. See Figure 8 for the location of this figure.

- Lupa and Ufipa faults follow pre-rift basement structures identified by alternating low and high magnetic anomalies
- The orientation of Precambrian basement structures impacts strain localisation within rift border faults
- Continuous lineaments inferred from magnetic data analyses suggest a direct link between the Lupa and Livingstone faults (Rukwa and Nyasa lakes rift segments)
- Chisi shear zone continues in a NW-SE direction under the Lake-Beds sediments of the Rukwa Rift Basin

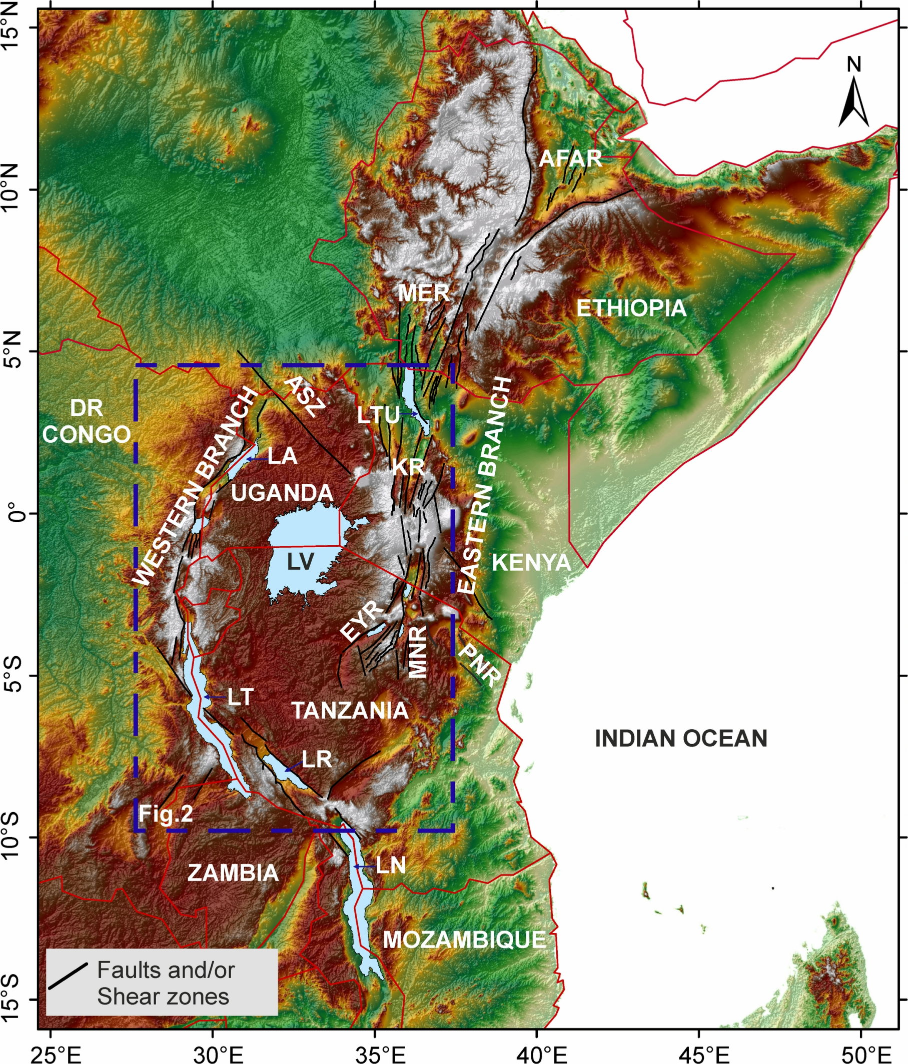

N
AFAR
MER
ETHIOPIA
ASZ
LTU
DR
CONGO
WESTERN BRANCH
LA
KR
UGANDA
EASTERN BRANCH
KENYA
LV
EYR
MNR
PNR
LT
TANZANIA
INDIAN OCEAN
LR
Fig.2
ZAMBIA
LN
MOZAMBIQUE
Faults and/or
Shear zones
15°N
10°N
5°N
0°
5°S
10°S
15°S
25°E
30°E
35°E
40°E
45°E
50°E

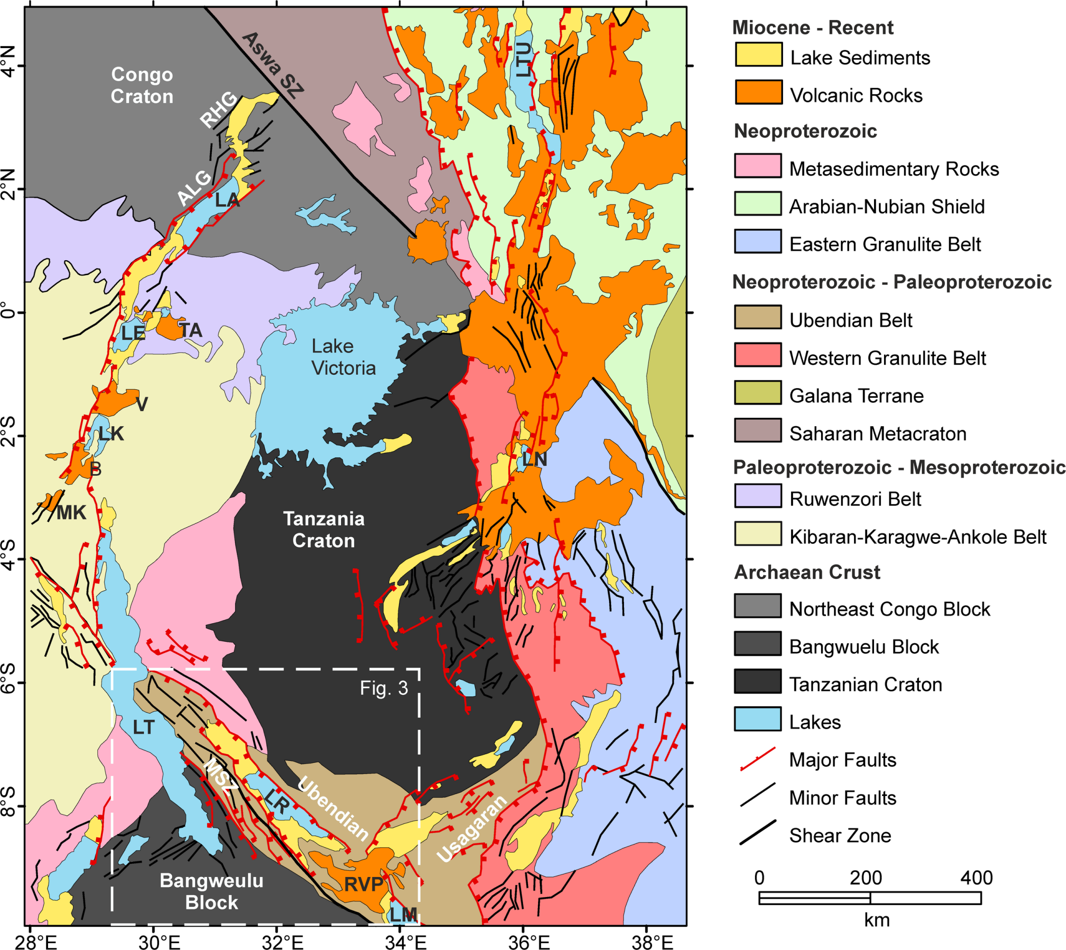

Miocene - Recent
Lake Sediments
Volcanic Rocks
Neoproterozoic
Metasedimentary Rocks
Arabian-Nubian Shield
Eastern Granulite Belt
Neoproterozoic - Paleoproterozoic
Ubendian Belt
Western Granulite Belt
Galana Terrane
Saharan Metacraton
Paleoproterozoic - Mesoproterozoic
Ruwenzori Belt
Kibaran-Karagwe-Ankole Belt
Archaean Crust
Northeast Congo Block
Bangwuelu Block
Tanzanian Craton
Lakes
Major Faults
Minor Faults
Shear Zone
0
200
400
km
Congo Craton
Aswa SZ
RHG
ALG
LA
LTU
LE
TA
Lake Victoria
V
LK
B
MK
LN
Tanzania Craton
Fig. 3
LT
MSZ
LR
Ubendian
Usagaran
RVP
Bangweulu Block
LM
4°N
2°N
0°
2°S
4°S
6°S
8°S
28°E
30°E
32°E
34°E
36°E
38°E

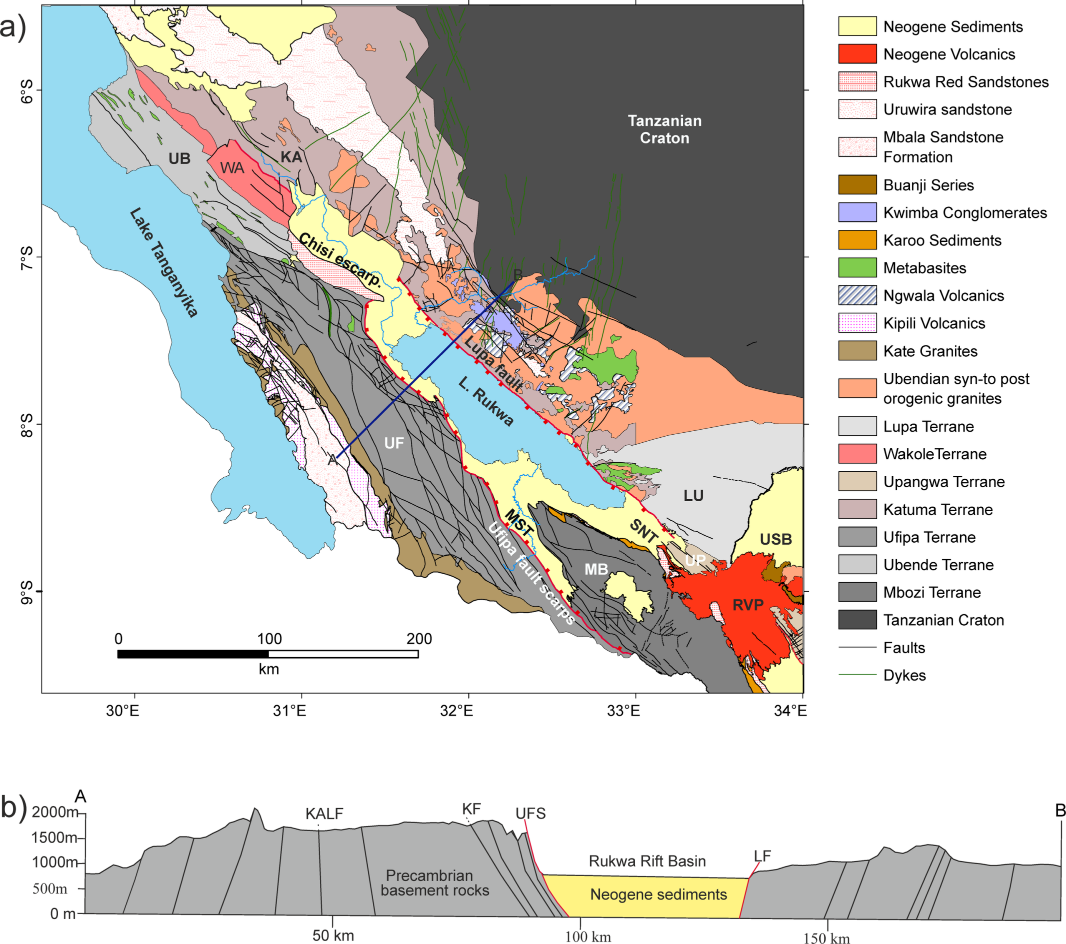

a)
b)
Neogene Sediments
Neogene Volcanics
Rukwa Red Sandstones
Uruwira sandstone
Mbala Sandstone Formation
Buanji Series
Kwimba Conglomerates
Karoo Sediments
Metabasites
Ngwala Volcanics
Kipili Volcanics
Kate Granites
Ubendian syn-to post orogenic granites
Lupa Terrane
WakoleTerrane
Upangwa Terrane
Katuma Terrane
Ufipa Terrane
Ubende Terrane
Mbozi Terrane
Tanzanian Craton
Faults
Dykes
Tanzanian Craton
Lake Tanganyika
Chisi escarp.
Lupa fault
L. Rukwa
Ufipa fault scarps
UB
WA
KA
UF
MST
SNT
MB
LU
UP
USB
RVP
A
B
0
100
200
km
6°S
7°S
8°S
9°S
30°E
31°E
32°E
33°E
34°E
A
B
2000m
1500m
1000m
500m
0 m
KALF
KF
UFS
LF
Rukwa Rift Basin
Precambrian basement rocks
Neogene sediments
50 km
100 km
150 km

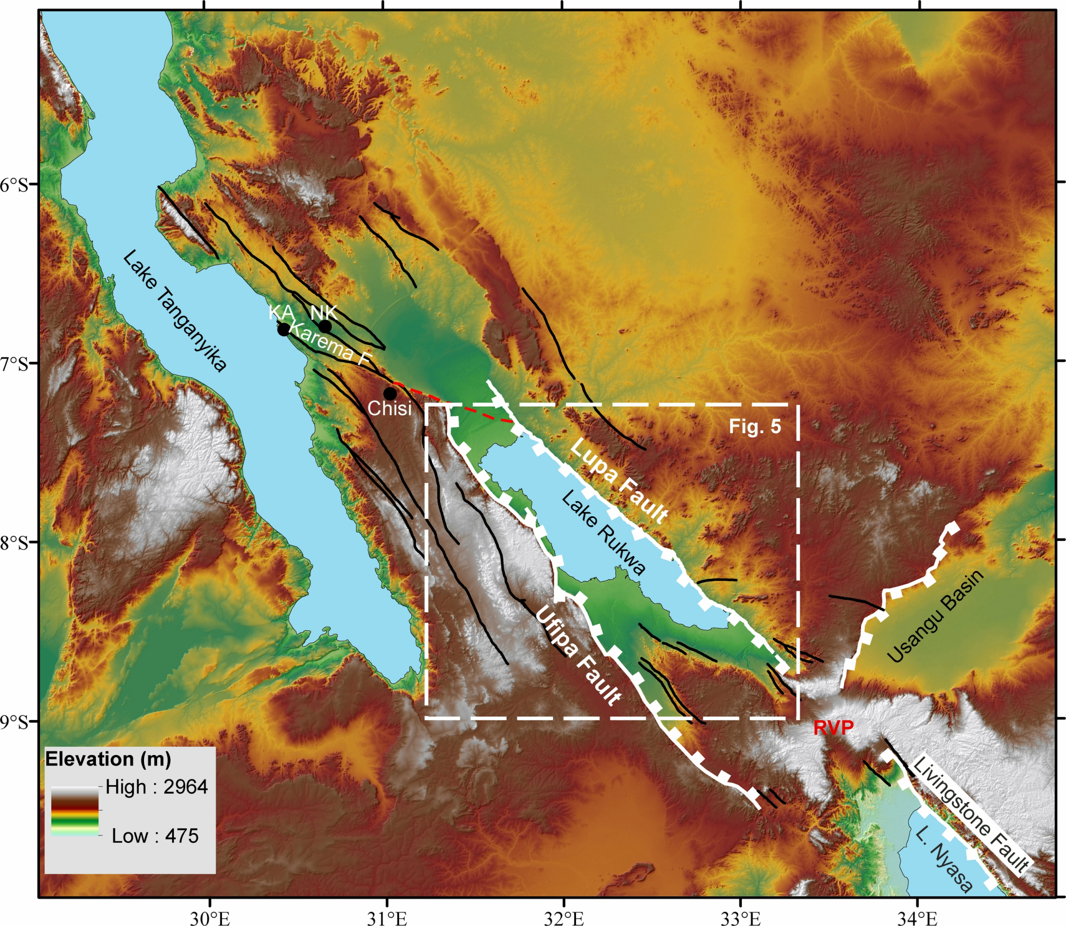

6°S
7°S
8°S
9°S
30°E
31°E
32°E
33°E
34°E
Lake Tanganyika
KA
NK
Karema F
Chisi
Fig. 5
Lupa Fault
Lake Rukwa
Ufipa Fault
Usangu Basin
RVP
Livingstone Fault
L. Nyasa
Elevation (m)
High : 2964
Low : 475

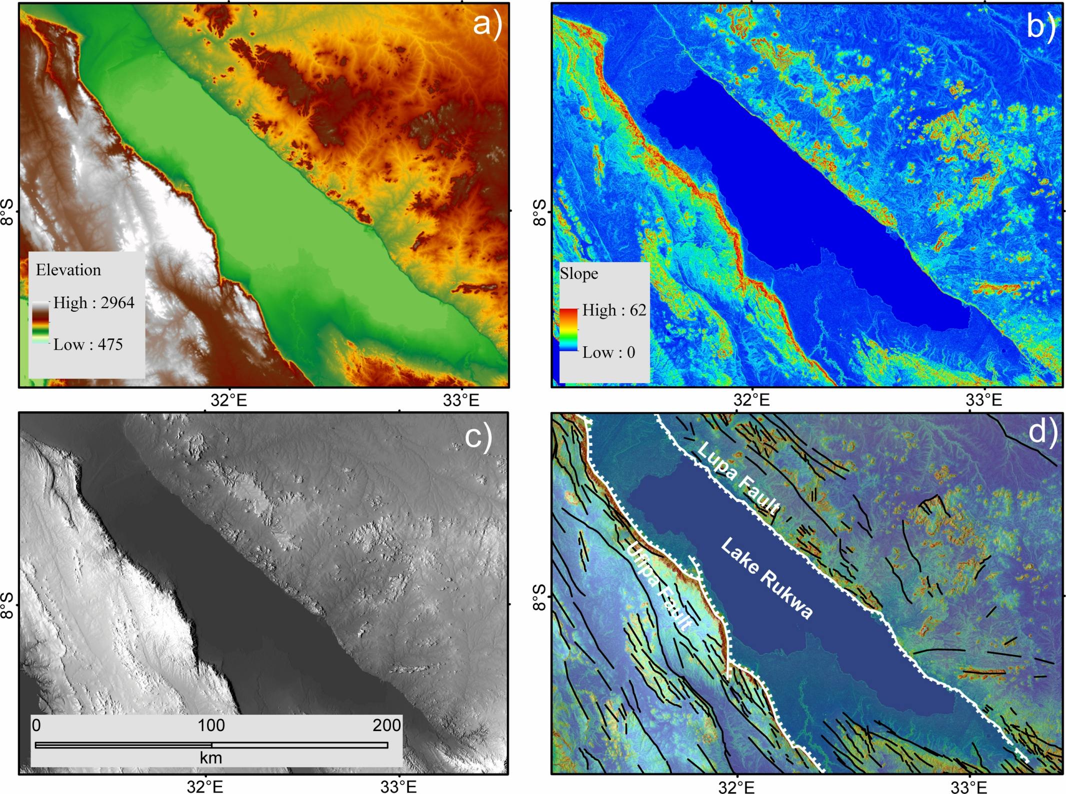
a)
Elevation
High : 2964
Low : 475
b)
Slope
High : 62
Low : 0
c)
0
100
200
km
d)
Lupa Fault
Lake Rukwa
Ufipa Fault
8°S
32°E
33°E

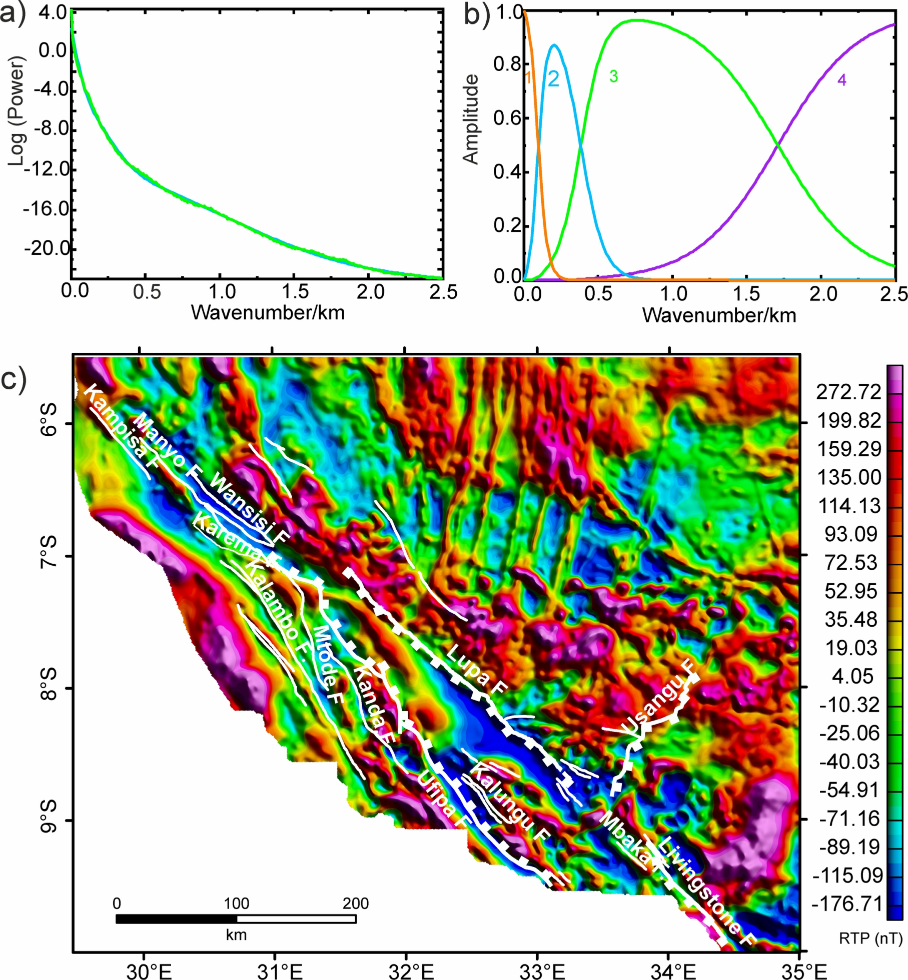

a)
Log (Power)
4.0
0.0
-4.0
-8.0
-12.0
-16.0
-20.0
0.0
0.5
1.0
1.5
2.0
2.5
Wavenumber/km
b)
Amplitude
1.0
0.8
0.6
0.4
0.2
0.0
1
2
3
4
Wavenumber/km
c)
6°S
7°S
8°S
9°S
30°E
31°E
32°E
33°E
34°E
35°E
Kampisa F
Manyo F
Wansisi F
Karema F
Kalambo F
Mtode F
Kanda F
Lupa F
Usangu F
Ufipa F
Kalungu F
Mbaka F
Livingstone F
0
100
200
km
272.72
199.82
159.29
135.00
114.13
93.09
72.53
52.95
35.48
19.03
4.05
-10.32
-25.06
-40.03
-54.91
-71.16
-89.19
-115.09
-176.71
RTP (nT)

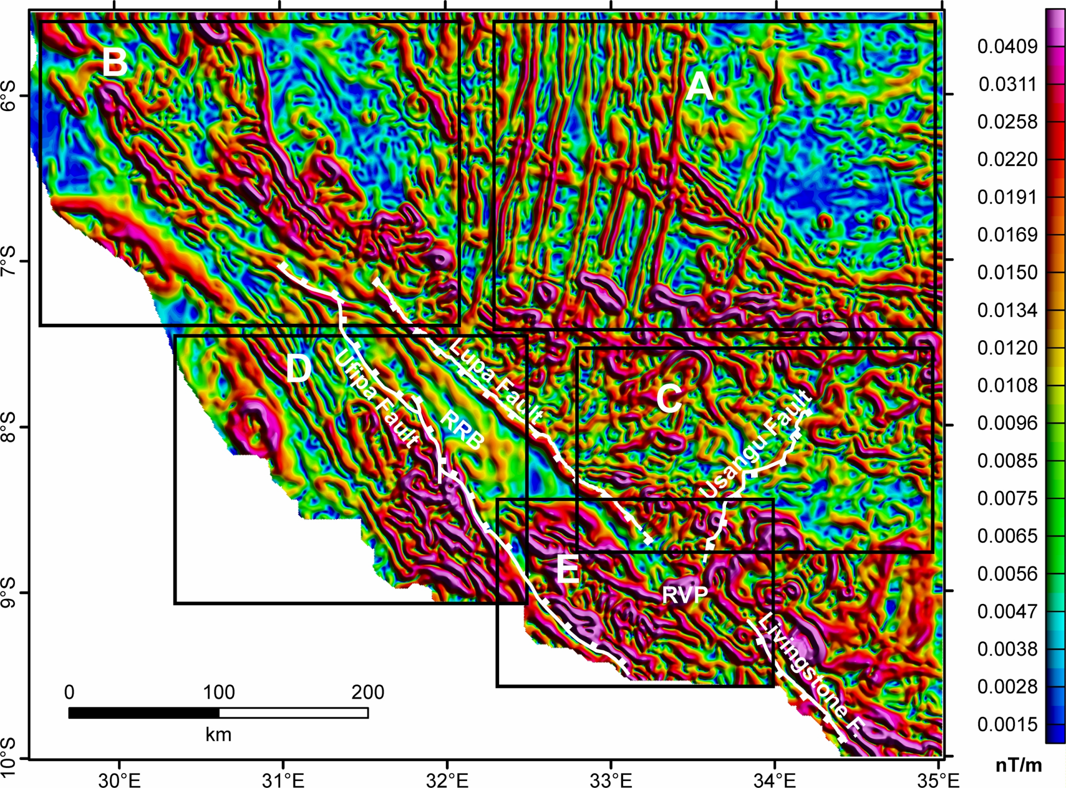

B
A
D
C
E
Lupa Fault
Ufipa Fault
RRB
Usangu Fault
RVP
Livingstone F.
0
100
200
km
6°S
7°S
8°S
9°S
10°S
30°E
31°E
32°E
33°E
34°E
35°E
0.0409
0.0311
0.0258
0.0220
0.0191
0.0169
0.0150
0.0134
0.0120
0.0108
0.0096
0.0085
0.0075
0.0065
0.0056
0.0047
0.0038
0.0028
0.0015
nT/m

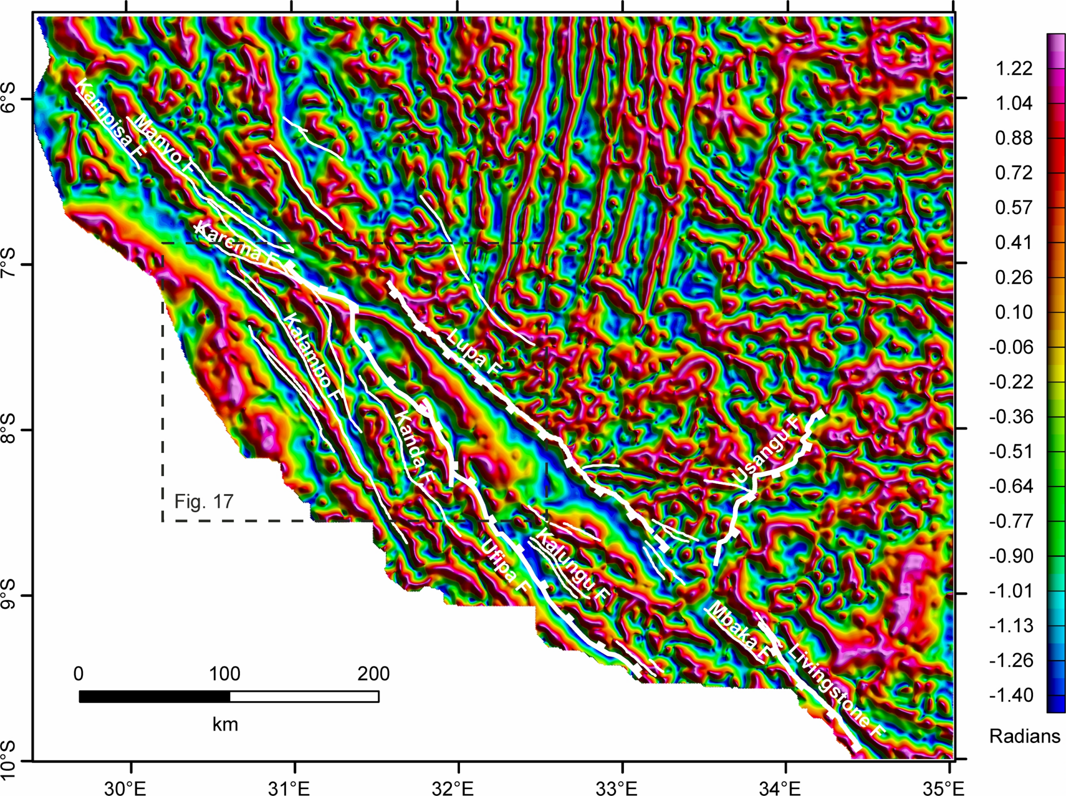

Kampisa F
Manyo F
Karema F
Kalambo F
Lupa F
Kanda F
Ufipa F
Kalungu F
Usangu F
Mbaka F
Livingstone F
Fig. 17
0
100
200
km
6°S
7°S
8°S
9°S
10°S
30°E
31°E
32°E
33°E
34°E
35°E
1.22
1.04
0.88
0.72
0.57
0.41
0.26
0.10
-0.06
-0.22
-0.36
-0.51
-0.64
-0.77
-0.90
-1.01
-1.13
-1.26
-1.40
Radians

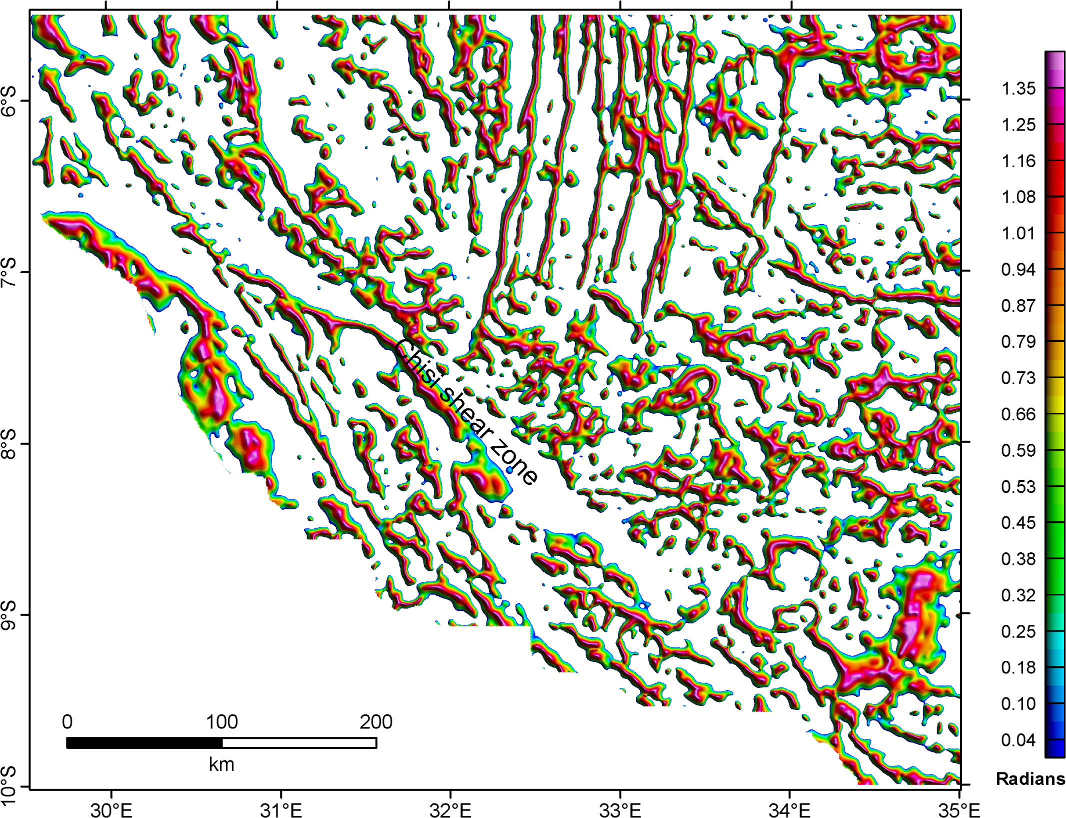

6°S
7°S
8°S
9°S
10°S
30°E
31°E
32°E
33°E
34°E
35°E
Chisi shear zone
0
100
200
km
1.35
1.25
1.16
1.08
1.01
0.94
0.87
0.79
0.73
0.66
0.59
0.53
0.45
0.38
0.32
0.25
0.18
0.10
0.04
Radians

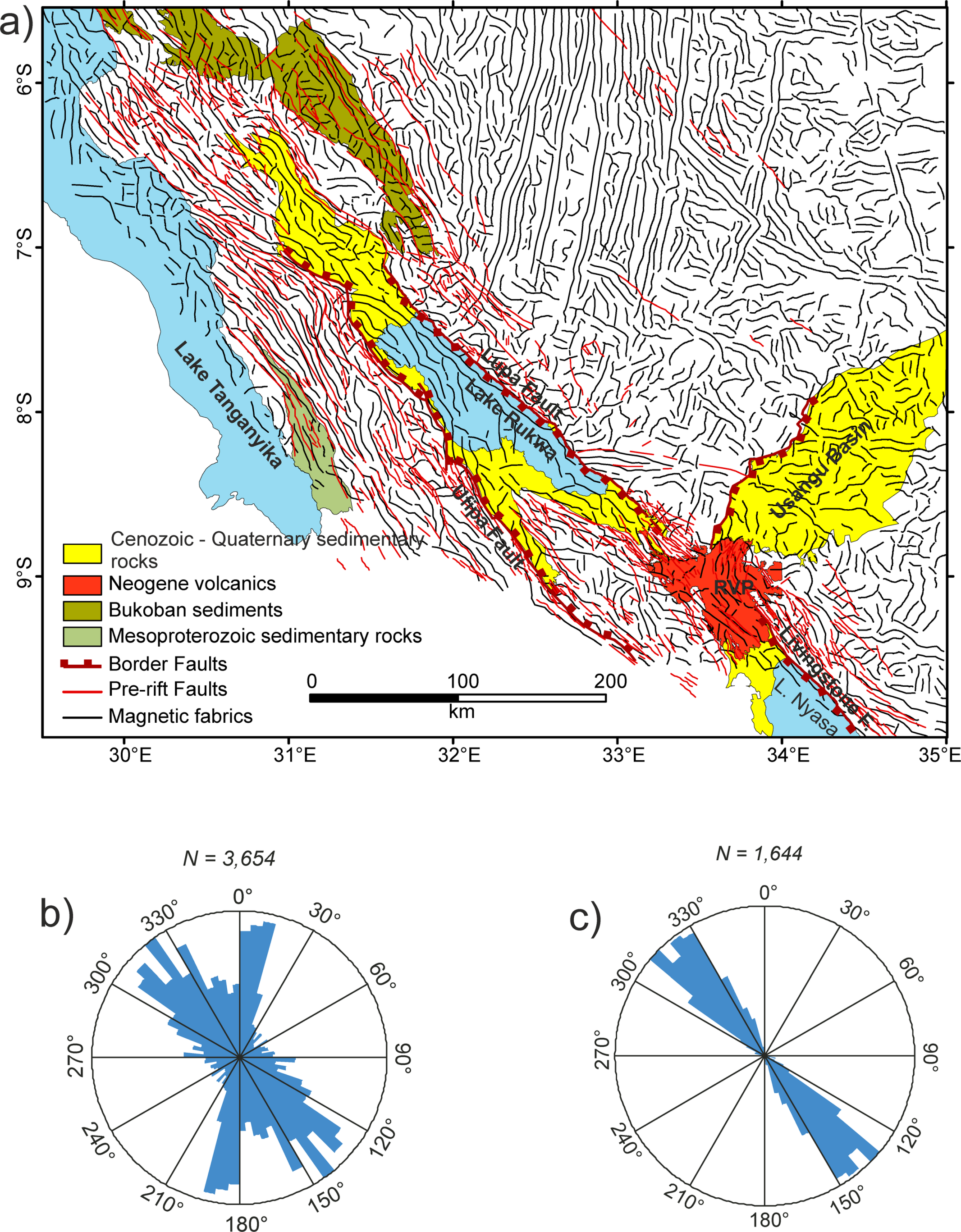
a)
6°S
7°S
8°S
9°S
30°E
31°E
32°E
33°E
34°E
35°E
Lake Tanganyika
Lake Rukwa
Lupa Fault
Ufipa Fault
Usangu Basin
RVP
Livingstone F.
L. Nyasa
Cenozoic - Quaternary sedimentary rocks
Neogene volcanics
Bukoban sediments
Mesoproterozoic sedimentary rocks
Border Faults
Pre-rift Faults
Magnetic fabrics
0
100
200
km
b)
N = 3,654
c)
N = 1,644
0°
30°
60°
90°
120°
150°
180°
210°
240°
270°
300°
330°

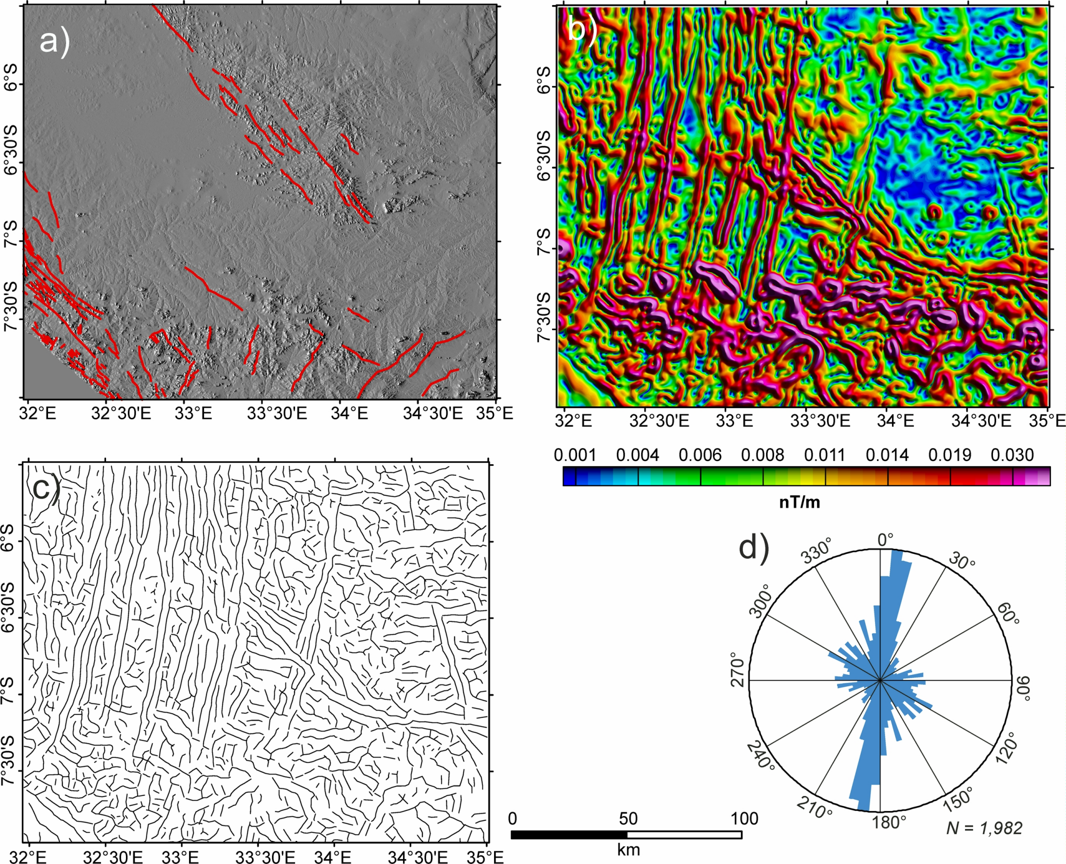

a)
b)
c)
d)
6°S
6°30'S
7°S
7°30'S
32°E
32°30'E
33°E
33°30'E
34°E
34°30'E
35°E
0.001
0.004
0.006
0.008
0.011
0.014
0.019
0.030
nT/m
0°
30°
60°
90°
120°
150°
180°
210°
240°
270°
300°
330°
N = 1,982
0
50
100
km

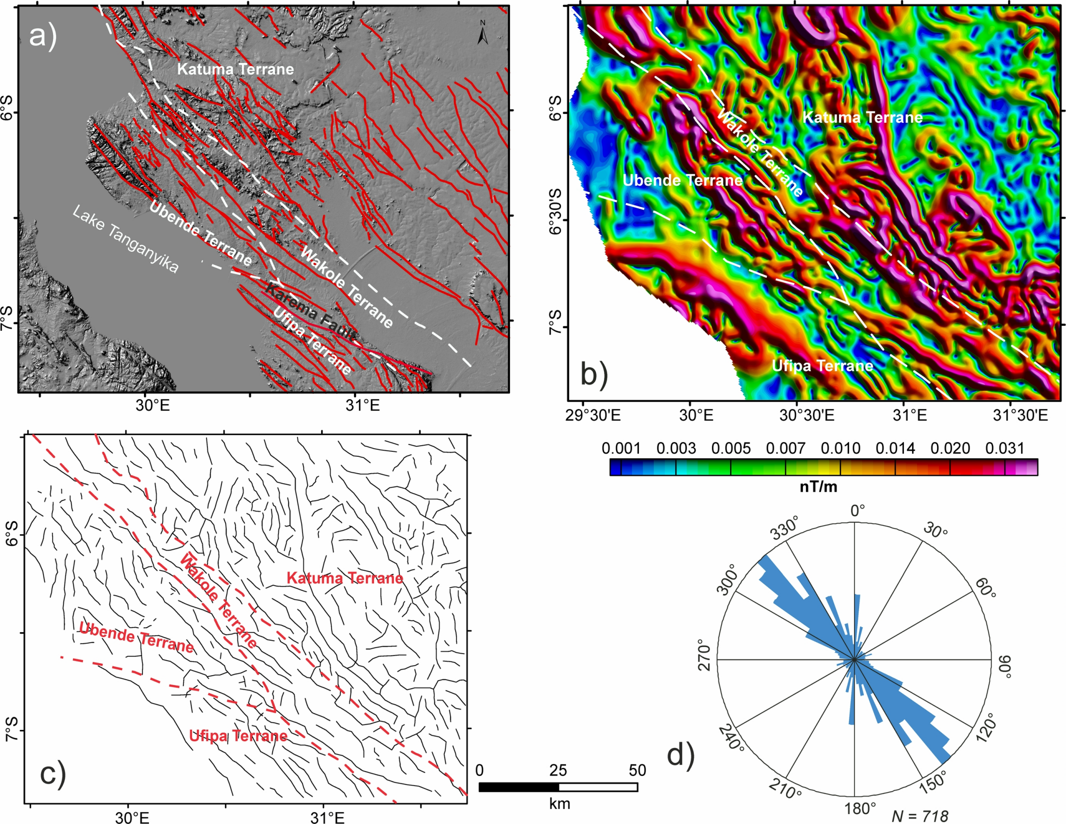

a)
Katuma Terrane
Ubende Terrane
Lake Tanganyika
Wakole Terrane
Karema Fault
Ufipa Terrane
6°S
7°S
30°E
31°E
b)
Katuma Terrane
Wakole Terrane
Ubende Terrane
Ufipa Terrane
6°S
6°30'S
7°S
29°30'E
30°E
30°30'E
31°E
31°30'E
0.001
0.003
0.005
0.007
0.010
0.014
0.020
0.031
nT/m
c)
Wakole Terrane
Katuma Terrane
Ubende Terrane
Ufipa Terrane
6°S
7°S
30°E
31°E
0
25
50
km
d)
0°
30°
60°
90°
120°
150°
180°
210°
240°
270°
300°
330°
N = 718

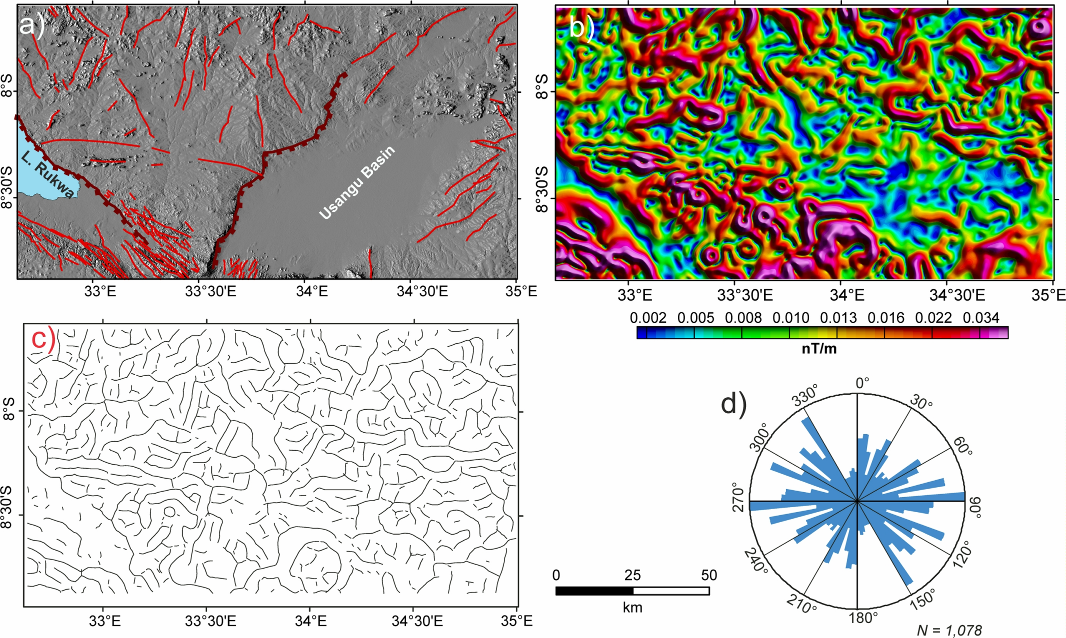

a)
L. Rukwa
Usangu Basin
8°S
8°30'S
33°E
33°30'E
34°E
34°30'E
35°E
b)
0.002
0.005
0.008
0.010
0.013
0.016
0.022
0.034
nT/m
c)
d)
0°
30°
60°
90°
120°
150°
180°
210°
240°
270°
300°
330°
N = 1,078
0
25
50
km

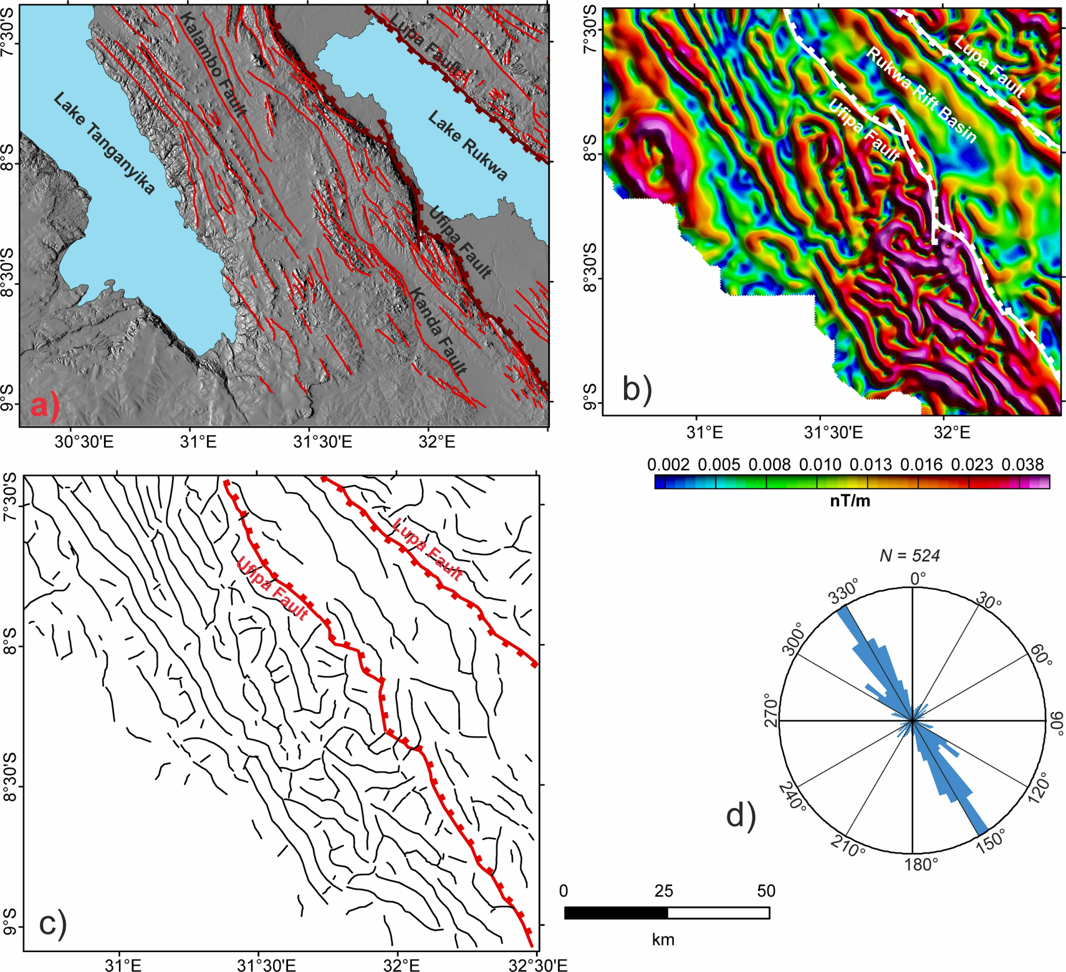

a)
Lake Tanganyika
Lake Rukwa
Kalambo Fault
Lupa Fault
Ufipa Fault
Kanda Fault
7°30'S
8°S
8°30'S
9°S
30°30'E
31°E
31°30'E
32°E
b)
Lupa Fault
Rukwa Rift Basin
Ufipa Fault
0.002 0.005 0.008 0.010 0.013 0.016 0.023 0.038
nT/m
c)
Ufipa Fault
Lupa Fault
32°30'E
0 25 50
km
d)
N = 524
0°
30°
60°
90°
120°
150°
180°
210°
240°
270°
300°
330°

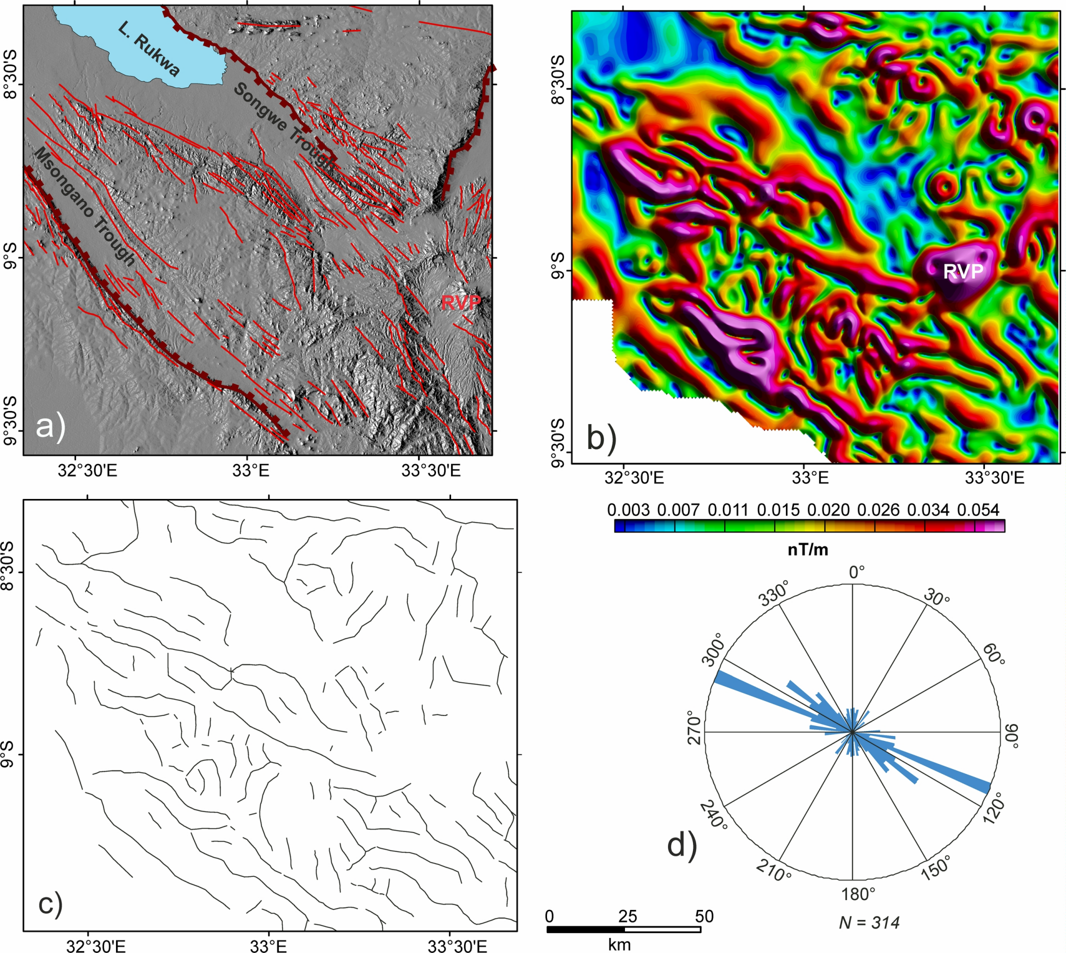

L. Rukwa
Songwe Trough
Msongano Trough
RVP
a)
b)
c)
d)
8°30'S
9°S
9°30'S
32°30'E
33°E
33°30'E
0.003 0.007 0.011 0.015 0.020 0.026 0.034 0.054
nT/m
0°
30°
60°
90°
120°
150°
180°
210°
240°
270°
300°
330°
N = 314
0 25 50
km

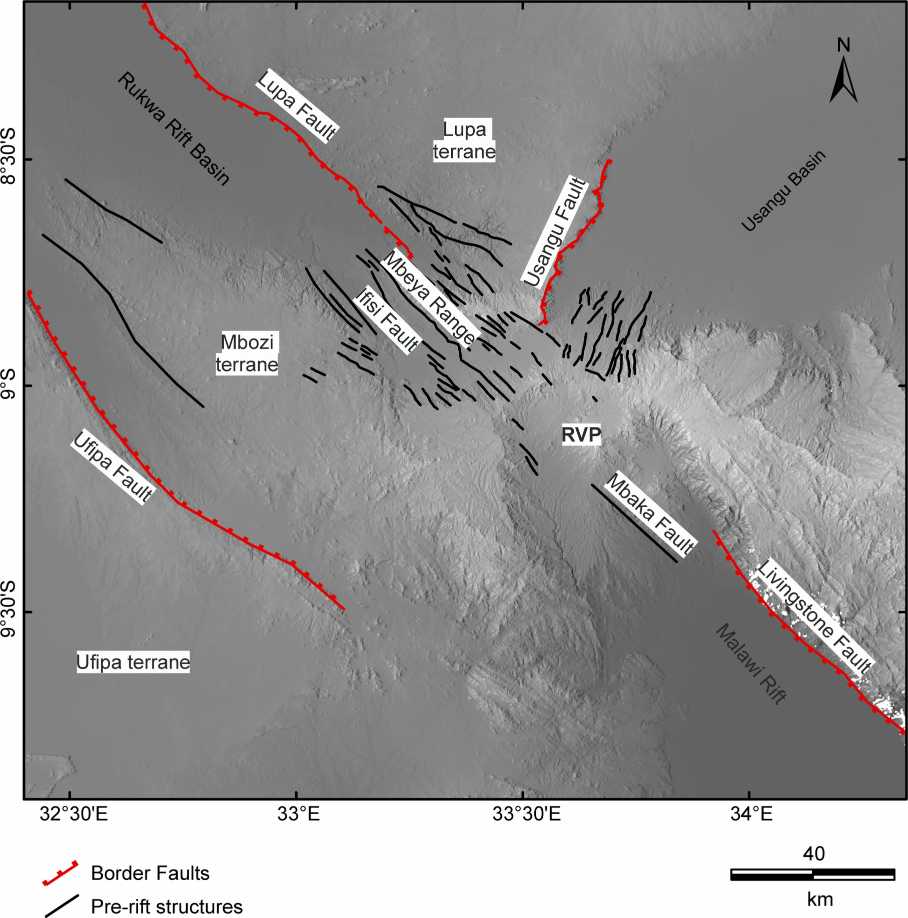
N
Rukwa Rift Basin
Lupa Fault
Lupa terrane
Usangu Fault
Usangu Basin
Mbeya Range
Ifisi Fault
Mbozi terrane
RVP
Ufipa Fault
Mbaka Fault
Livingstone Fault
Malawi Rift
Ufipa terrane
8°30'S
9°S
9°30'S
32°30'E
33°E
33°30'E
34°E
40
km
Border Faults
Pre-rift structures

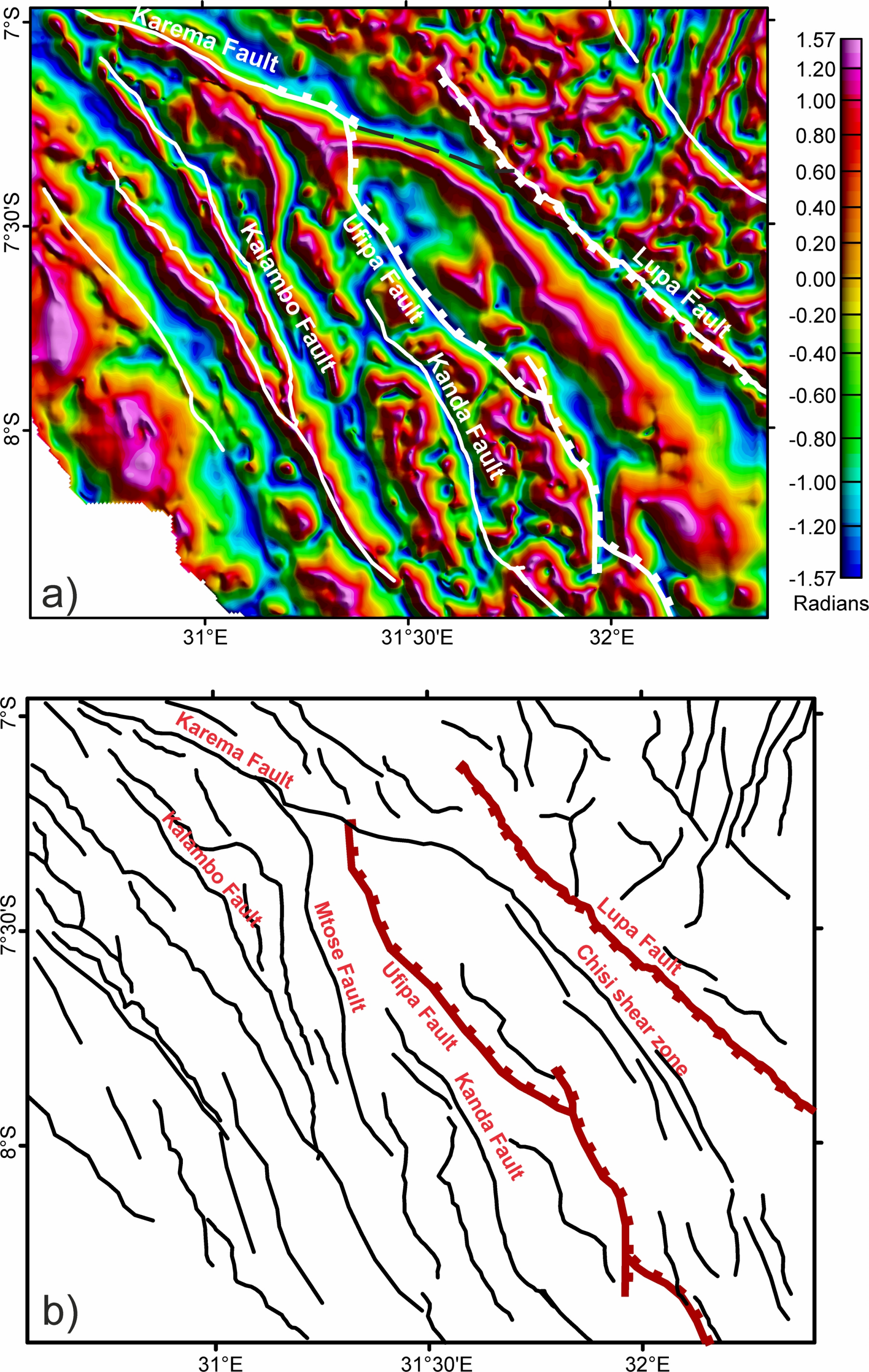

7°S
7°30'S
8°S
31°E
31°30'E
32°E
Karema Fault
Kalambo Fault
Ufipa Fault
Kanda Fault
Lupa Fault
1.57
1.20
1.00
0.80
0.60
0.40
0.20
0.00
-0.20
-0.40
-0.60
-0.80
-1.00
-1.20
-1.57
Radians
a)
Karema Fault
Kalambo Fault
Mtose Fault
Ufipa Fault
Kanda Fault
Lupa Fault
Chisi shear zone
b)